

Lawrence University

Lux

---

Lawrence University Honors Projects

---

2023

## Mechanism of PTH $Ca^{2+}$ Sensing on G-Protein Interactions with PTH1R

Difei Jiang

Follow this and additional works at: <https://lux.lawrence.edu/luhp>



Part of the [Chemistry Commons](#)

© Copyright is owned by the author of this document.

---

This Honors Project is brought to you for free and open access by Lux. It has been accepted for inclusion in Lawrence University Honors Projects by an authorized administrator of Lux. For more information, please contact [colette.brautigam@lawrence.edu](mailto:colette.brautigam@lawrence.edu).



Honor Thesis

MECHANISM OF PTH  $Ca^{2+}$   
SENSING ON G-PROTEIN  
INTERACTIONS WITH PTH1R

Difei Jiang

May.1st.2023



## Abstract

Parathyroid hormone 1 receptor (PTH1R) is a family-B GPCR that plays a crucial role in bone remodeling. Previous studies show extracellular  $\text{Ca}^{2+}$  is a positive allosteric modulator for one PTH1R ligand, parathyroid hormone (PTH), which is approved by US FDA to treat severe osteoporosis. Moreover, PTH residues E19 & E22 have shown to be involved in  $\text{Ca}^{2+}$  sensing. However, the effects of PTH  $\text{Ca}^{2+}$  sensing on intracellular G-protein binding are unknown. Here, we used FRET-based SPASM sensors to study the interaction between PTH1R and different  $G_{\alpha}$  peptides. SPASM sensors, which are isolated in native HEK293T membranes through optimized protocol, contain PTH1R followed by the acceptor fluorophore, a flexible linker, the donor fluorophore, and a peptide from a  $G_{\alpha}$  subunit that mimics the interaction of the full G-protein heterotrimer. In the current study, two SPASM sensor preparation methods, Giant Plasma Membrane Vesiculation and native membrane preparation, were employed. The quality and integrality of the SPASM sensors isolated through each method were evaluated and compared to one another. We performed FRET experiments to quantify the activation of different  $G_{\alpha}$  isoforms by PTH and its  $\text{Ca}^{2+}$  sensing mutant, PTHE19AE22A. PTH binding to PTH1R SPASM sensors causes differential interactions between PTH1R and the  $G_s$ ,  $G_q$  and  $G_i$  peptides. PTHE19AE22A activation of PTH1R-SPASM sensors leads to distinct interaction profiles between each G-peptide isoforms, which were further modulated by the presence of extracellular  $\text{Ca}^{2+}$ . Quantifying the differential activation of the specific  $G_{\alpha}$  isoforms by PTH and PTHE19AE22A in the presence and absence of  $\text{Ca}^{2+}$  will delineate mechanistic details of PTH1R activation and its role in bone-related diseases. Further, understanding the extracellular  $\text{Ca}^{2+}$  modulation of PTH signaling will provide insight for developing treatments for chronic hypocalcemia associated with hypoparathyroidism, while uncovering PTH1R novel regulation in bone remodeling.

## Introduction

### GPCRs (G-Protein-Coupled Receptors)

G-protein-coupled receptors (GPCRs) are one of the largest protein superfamilies including more than 800 distinct human cell surface receptors, with approximately 450 sensory receptors engaging in olfaction, pheromone signaling, light perception, and taste.<sup>1</sup> The remaining non-sensory GPCRs are involved in cell-to-cell signaling and are targets for a large portion of current pharmaceutical development.<sup>2,3</sup> GPCRs remain the main mediators by which cells detect environmental stimuli through binding of extracellular ligands, and they enable cell-to-cell communication by stimulating a series of downstream signals.<sup>4,5</sup> All GPCRs exhibit a characteristic structure of seven transmembrane  $\alpha$ -helices and are activated by a variety of extracellular ligands, including hormones, large proteins, ions, lipids, neurotransmitters, sensory stimuli, and photons.<sup>1</sup> In addition to ligand-induced activation, GPCRs can also be stimulated by cell membrane lipid composition, tension, voltage, and fluidity of the membrane.<sup>6-9</sup> The function of GPCRs is also regulated by common ions such as sodium and cellular pH level.<sup>10,11</sup>

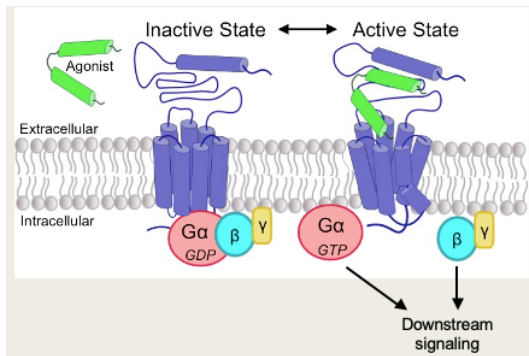


Figure 1: Schematic of GPCR (purple) inactive and active states. The inactive state has no agonist/ligand (green) bound on the extracellular side but has heterotrimeric G-proteins consisting of  $G_{\alpha}$ ,  $G_{\beta}$ , and  $G_{\gamma}$  subunits as a single unit bound on the cytoplasmic side;  $G_{\alpha}$  is bound to GDP. Upon agonist/ligand binding, GPCR shifts to the active state, GDP is exchanged with GTP, and  $G_{\alpha}$  dissociates from  $G_{\beta\gamma}$  which can each initiate different signaling cascade separately.

A single GPCR can be activated by multiple ligands through distinct conformational changes when different ligands bind. The conformational changes of the receptor then lead to the activation of specific heterotrimeric G-proteins that associate with the GPCR intracellularly. Those G-proteins are comprised of  $G_{\alpha}$ ,  $G_{\beta}$ , and  $G_{\gamma}$  subunits that are bound together prior to activation. The  $G_{\alpha}$  subunit binds guanosine diphosphate (GDP) in its inactive state. Once activated, the  $G_{\alpha}$  subunit exchanges the bound nucleotide, GDP, with guanosine triphosphate (GTP). The nucleotide exchange induces the disassociation of the  $G_{\alpha}$  subunit from the  $G_{\beta\gamma}$  subunits. The dissociated subunits activate signaling cascades that produce secondary messengers and induce changes in cellular synthesis of a variety of compounds, such as calcium, cyclic adenosine monophosphate

(cAMP), or diacylglycerol (Figure 1).<sup>1</sup> Second messengers change gene expression in the cell by entering the nucleus and binding to promoters or transcription factors of target genes.

The specific isoform of the activated  $G_{\alpha}$  subunit determines which intracellular pathway is activated. So far, 16  $G_{\alpha}$  have been identified that are encoded by the human genome, which are categorized into four subfamilies including  $G_{\alpha_s}$ ,  $G_{\alpha_i/o}$ ,  $G_{\alpha_q/11}$ , and  $G_{\alpha_{12/13}}$ .<sup>4</sup>  $G_{\alpha_s}$  and  $G_{\alpha_i}$  regulate intracellular concentration of cyclic adenosine monophosphate (cAMP) through activation and inhibition of adenylyl cyclase, respectively. Activated  $G_{\alpha_s}$  increases intracellular cAMP level by engaging the  $G_{\alpha_s}$ /adenylyl cyclase/cAMP/protein kinase A (PKA) pathway, whereas  $G_{\alpha_i}$  decreases intracellular cAMP level by inhibiting adenylyl cyclase activity.<sup>12</sup>  $G_{\alpha_q}$  increases intracellular levels of  $Ca^{2+}$  and inositol trisphosphate ( $IP_3$ ) by activating effector phospholipase C- $\beta$  isozymes through the  $G_{\alpha_q}$ /phospholipase C (PLC) $\beta$ /inositol trisphosphate ( $IP_3$ )/intracellular  $Ca^{2+}$ /protein kinase C (PKC) pathway.<sup>13</sup> Lastly,  $G_{\alpha_{12/13}}$ -phospholipase D/RhoA pathway has been known to be involved in the activation of RhoGTPases which can result in various intracellular signaling such as rearrangement of actine cytoskeleton, embryogenesis, and gene transcription upon activation.<sup>14</sup>

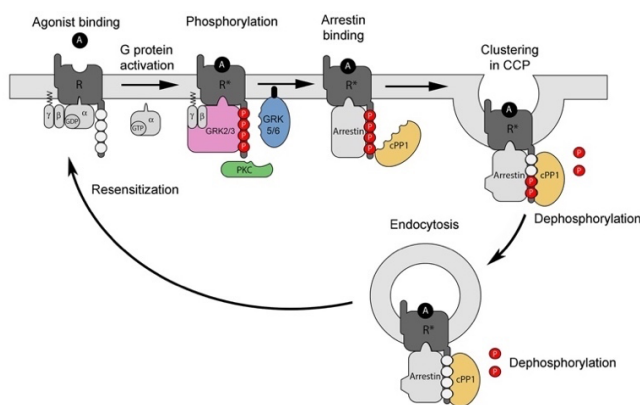


Figure 2: Schematic representation of the G-protein-coupled receptor phosphorylation/dephosphorylation cycle. GRK, G-protein-coupled receptor kinase; PKC, protein kinase C; cPP1, catalytic subunit of protein phosphatase 1; R\*, activated GPCR; CCP, clathrin-coated pit.<sup>52</sup>

endocytosis machinery through clathrin-coated pits, in which plasma membrane coated with clathrin wraps around the receptor and leads to formation of vesicle buds. As newly formed vesicles mature, the membrane-bound receptors are internalized as intracellular vesicles and targeted to the endosome either for degradation or dephosphorylation by the catalytic subunit of protein phosphatase 1 (cPP1) (Figure 2).<sup>16</sup> The dephosphorylation of GPCR enables the receptor to be recycled back to plasma membrane for another round of signaling.

Canonically, ligand and G-protein interactions induce the active state of a GPCR. Thus, the ternary complex model of GPCR interactions included two receptor conformations, with an inactive receptor state in equilibrium with an active receptor state.<sup>17</sup> Agonists and partial agonists stimulate activation of the heterotrimeric G-proteins by shifting the equilibrium toward the active state, whereas inverse agonists can suppress activation of the heterotrimeric G-proteins by shifting the equilibrium to the inactive state.<sup>1</sup> Using advanced scientific techniques such as NMR spectroscopy, double electron-electron resonance spectroscopy, X-ray crystallography, single molecule fluorescence, molecular dynamics experiments, and nanobodies for studying protein structures, recent studies reveal the conformational dynamics that govern GPCR structure and activation.<sup>18–22</sup> Rather than discrete on and off states as previously thought, these studies show GPCRs sample distinct conformations in an ensemble. Ligand binding increases an individual receptor's conformational complexity by stabilizing distinct receptor states in the conformational ensemble. These stabilized receptor states further result in selective activation of  $G_{\alpha}$  isoforms and their associated signaling pathways. The conformational dynamic of the GPCRs, therefore, results in functional complexity of GPCRs.

The signaling cascades activated by GPCRs are terminated upon phosphorylation at the receptor's consensus phosphorylation sites which interfere with receptor-G-protein coupling.<sup>15</sup> Specifically, when GPCRs are activated, G-protein-coupled receptor kinase (GRK) is also activated. GRK, along with PKA and protein kinase C (PKC), transfers one phosphate group from adenosine triphosphate (ATP) to GPCR. GPCR phosphorylation recruits  $\beta$ -arrestin, which binds intracellularly to the GPCR to prevent the interaction of the receptor to G-proteins. The binding of  $\beta$ -arrestin couples the receptor with

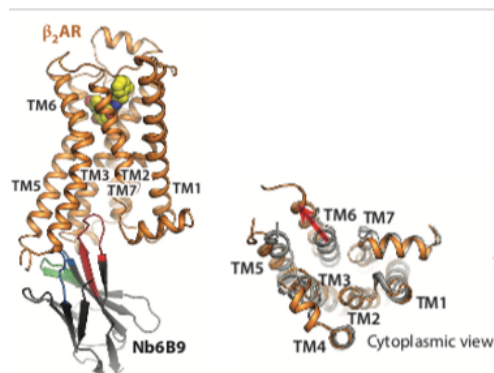


Figure 3 (Left): Active-state structures of agonist-bound, nanobody-stabilized GPCRs with seven transmembrane  $\alpha$ -helices (orange).

Figure 3 (Right): Cytoplasmic view comparing inactive (grey) and active receptors (colored), featuring outward displacement of TM6, inward movement of TM5, and rearrangement of TM7.<sup>1</sup>

of TM3, TM5, TM6, and intracellular loop (ICL) 2.<sup>5</sup>

The role of conformational ensembles in GPCR structure and function is best illustrated through a discussion of the  $\beta$ 2-adrenergic receptor ( $\beta$ 2-AR), one of the most well studied family-A GPCRs with conformational dynamics affect by both ligand and intracellular G-protein binding. Recent studies of crystallographic structures of  $\beta$ 2-AR inactive and active states revealed that the most notable conformational change upon activation of  $\beta$ 2-AR was a 9-11Å outward movement of transmembrane 6 (TM6) accompanied by a slight inward movement of TM5 and rearrangement of a motif in TM7 (Figure 3).<sup>1</sup> The outward motion of TM6 is stabilized by the C-terminal  $\alpha$ 5 helix of  $G_{\alpha_s}$ , the preferred G-protein isoform for  $\beta$ 2-AR coupling. The  $\alpha$ 5 helix inserts into a pocket in  $\beta$ 2-AR formed by cytoplasmic ends

With the foundational knowledge of conformational changes during the activation of  $\beta$ 2-AR established, further studies showed variation in the movement of TM6 upon binding of various orthostatic ligands.<sup>23</sup> The ligands tested range from inverse agonists which suppress basal activity of  $\beta$ 2-AR, to partial and full agonists that differentially promote  $\beta$ 2-AR-induced  $G_s$  activation, and neutral antagonists that prevent agonist-mediated activation. Utilizing single-molecule fluorescence resonance energy transfer imaging (smFRET), TM6 was labeled with a donor fluorescent probe and TM4 was labeled with an acceptor fluorescent probe, which enabled quantification of the distance between the two transmembrane helices. The further apart TM4 and TM6 moved, the more conformational change  $\beta$ 2-AR underwent on the cytoplasmic side where heterotrimeric G-proteins bind. Thus, the relative distance between the two helices indicated the conformational states sampled by the GPCR, with more active states and G-protein-bound states showing larger relative distances. For example,  $\beta$ 2-AR- $G_s$  complexes spent more time in active conformations when bound to more efficacious ligands, especially when no GDP or GTP nucleotide was present. Based on those observations, the study was able to conclude that more efficacious ligands preferentially promote GDP release to achieve nucleotide-free states. The nucleotide-free state promotes more rapid and efficient GTP loading to  $G_{\alpha_s}$  and enables more rapid dissociation of  $G_{\alpha_s}$  from  $\beta$ 2-AR. By lowering the rate-limiting conformation transition of TM6 from active state to inactive state, more efficacious ligands stimulate more rapid signaling. This study showed that distinct GPCR conformations depend on the efficacy of the bound ligand and the nucleotide state of the coupled G-protein, demonstrating the multiple possible conformations of the  $\beta$ 2-AR- $G_s$  complexes and further highlighting the conformational complexity of GPCRs.

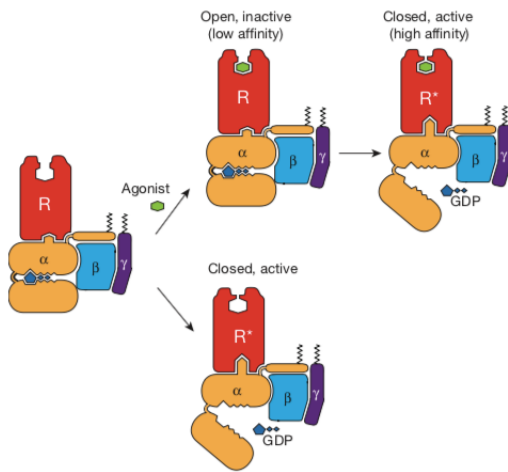


Figure 4: Schematic representation of G-protein-dependent high affinity agonist binding. Agonist binding promotes GDP release from the G-protein heterotrimer ( $G_{\alpha}$  ( $\alpha$ )  $G_{\beta\gamma}$  ( $\beta\gamma$ )) and allosteric change at the ligand binding site, restricting access to and egress from the ligand-binding site. Constitutive (basal) receptor activity may also activate the G-protein, releasing GDP and thereby stabilizing the nucleotide-free and closed conformation of the receptor in the absence of an agonist.<sup>5</sup>

the extracellular side of TM6, TM7 and ECL2. Additionally, the study analyzed the behavior of additional GPCRs including M2 muscarinic acetylcholine receptor (M2R) and the  $\mu$ -opioid receptor (MOPr) which revealed the shared mechanism of ligand association and disassociation at the ligand-binding site. M2R even exhibited a similar formation of the lid-like structure above the orthostatic ligand site. These findings suggest the allosteric effect of G-protein heterotrimers on the ligand is possibly a common mechanism shared among GPCRs, further supporting the need to understand changes in conformational dynamics of GPCRs.

These two studies highlight the complex conformational dynamics of  $\beta$ 2-AR and form the foundation for understanding the conformational dynamics of Parathyroid Hormone 1 Receptor (PTH1R), a family-B GPCR.

### PTH1R (Parathyroid Hormone 1 Receptor)

GPCRs' conformational complexity is not only induced by ligand efficacy but is influenced by intracellular G-protein binding. DeVree et al., (2016) revealed that intracellular G-protein binding allosterically impacts ligand binding to  $\beta$ 2-AR.<sup>5</sup> By utilizing a nanobody to stabilize the active state of  $\beta$ 2-AR, the study measured changes in ligand binding kinetics to active and inactive conformations of  $\beta$ 2-AR. G-protein binding to  $\beta$ 2-AR increases ligand affinity by causing the orthostatic ligand-binding site to close around the bound ligand, which is stabilized by insertion of the C-terminal helix of  $G_{\alpha}$  into the  $\beta$ 2-AR core in the absence of nucleotide GDP. This "closed"  $\beta$ 2-AR allosteric structural change is characterized by restricted access to and egress from the ligand-binding site and is also induced during constitutive/basal activity of  $\beta$ 2-AR even in the absence of a ligand (Figure 4). The study further observed the  $\beta$ 2-AR conformation with limited access to the ligand-binding site is formed by residues on

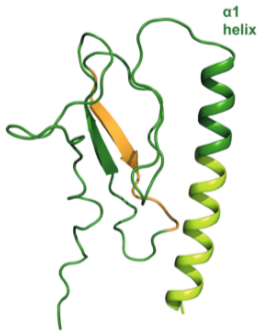


Figure 5: Schematic representation of PTH1R ECD. Two pairs of antiparallel  $\beta$ -strands form the core (yellow & green arrows). The long  $\alpha$ -helix on the N-terminus (spiral green) connects to the  $\beta$ -strands via extended loop.<sup>53</sup>

PTH1R is a family-B GPCR primarily expressed in bone, kidney, and mammary glands, where it plays a crucial role in both anabolic and catabolic bone remodeling. The PTH-receptor systems are evolutionarily ancient with findings suggesting that PTH receptors originated before the protostome-deuterostome divergence that occurred about 1 billion years ago.<sup>24</sup> Like other family B GPCRs, PTH1R possesses a characteristically large extracellular domain (ECD) necessary for hormone binding. The ECD has with six conserved cysteines that stabilize the overall structural fold through three disulfide bonds. The ECD of PTH1R is flat and oblong with its core comprised of secondary protein structures, including a pair of antiparallel  $\beta$  strands in center, a  $\beta$  hairpin between  $\beta$  strands 1 and 2, and a long  $\alpha$ -helix on the N-terminus (Figure 5).

The family-B GPCR subgroup consists of 15 distinct receptors, each typically binding to moderately sized, single-chain polypeptide ligands ranging from 30 to 40 amino acids. Unlike other family-B GPCRs, the two endogenous ligands of PTH1R, parathyroid hormone (PTH) and parathyroid hormone related hormone (PTHrP), are 84 amino acids and 141 amino acids in length, respectively.<sup>24</sup> However, residues 1-34 of each PTH1R ligand control the full binding and signaling activity, leaving potential biologic roles of the extended region after residue 34 on the C-terminus of the ligands unknown.<sup>25,26</sup> PTH maintains homeostatic levels of  $\text{Ca}^{2+}$ , phosphate, and active vitamin D levels in blood and extracellular fluids through the binding and activating of PTH1R, whereas PTHrP regulates growth in bone and mammary glands tissues. Both hormones bind PTH1R following the two-site model.<sup>27</sup> First, the C-terminal peptide fragment of PTH (residues 15-34) interacts tightly with the N-terminal ECD of PTH1R. Then, the N-terminus associates with the transmembrane domain (TMD) of PTH1R with slower kinetics and weaker affinity (Figure 6). The full peptide binding triggers a conformational change in PTH1R, leading to receptor activation, G-protein coupling, and intracellular signaling cascades. PTH1R activation depends on changes in TMD due to interactions with PTH residue glutamate (E) 4 and on interactions of PTH residues 1-3 with receptor TM6.<sup>27</sup> Similar to PTH, PTHrP binds through its C-terminus and signals through its N-terminus. Sequence alignment of PTH and PTHrP shows 8

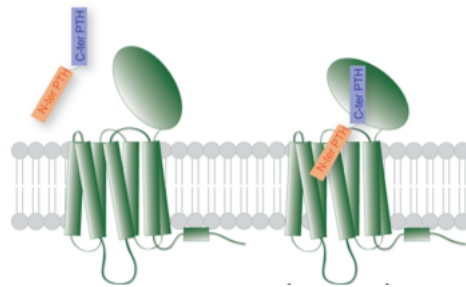


Figure 6: Schematic representation of PTH binding to PTH1R. The C-terminal fragment of PTH couples to the extracellular domain of the receptor, while the N-terminal part engages the transmembrane domain of the receptor.<sup>53</sup>

out of 13 identical amino acids in the N-terminus and two identical amino acids, arginine-20 and leucine-24, in 15-34 region (Figure 7).<sup>24</sup>

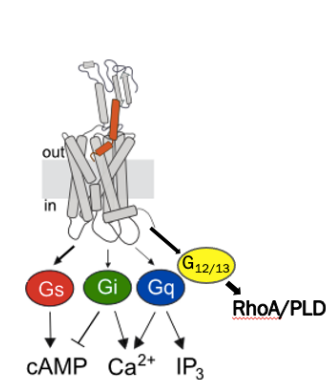
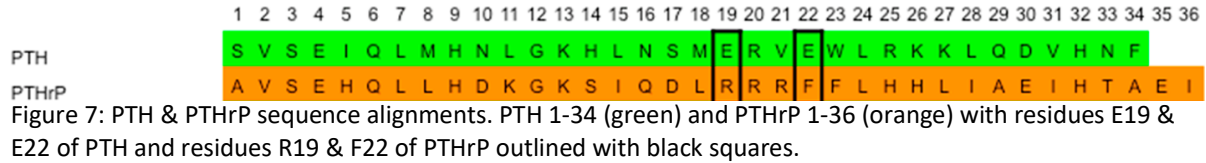


Figure 8: Ligand activation and second messengers signaling of PTH1R.

Upon ligand binding, PTH1R undergoes structural change involving outward movement of TM3 and TM6, inducing a sharp kink in the middle of TM6.<sup>27</sup> The opening of the TM6 cytosolic cavity allows the  $\alpha 5$  helix of  $G_{\alpha}$  at the C-terminus to insert, activating  $G_{\alpha}$  and distinct isoform-dependent signaling cascades (Figure 8).<sup>28</sup> Amino acids in intracellular loops (ICL) and on the intracellular side of the TMD contribute to the specificity of G-protein coupling and tailor PTH1R to signal through certain pathways when mutated. For example, signaling through  $G_{\alpha s}$  and  $G_{\alpha q}$  pathways was diminished when a lysine in the ICL3 was mutated to alanine; whereas mutation in ICL2 from lysine to glutamate tailored PTH1R to signal through  $G_{\alpha s}$  instead of the  $G_{\alpha q}$  pathway.<sup>29,30</sup> In addition, the hormone sequence also affects G-

protein coupling with residue one of both PTH and PTHrP involved in activating  $G_{\alpha q}$  signaling. Specifically, mutations in residue one of PTH and PTHrP decrease the activation of the  $G_{\alpha q}$  pathway while sustaining good potency for the  $G_{\alpha s}$  pathway.<sup>24</sup>

Consistent with other GPCRs, PTH1R is highly structurally dynamic and samples a variety of conformations stabilized by specific ligands to activate certain intracellular signaling pathways. Before the full-length structure of PTH1R was determined, previous studies found PTH1R formed two distinctive complexes,  $R^0$  and  $R^G$ , which differ in their interactions with PTH and PTHrP.<sup>24</sup> PTH binds with high affinity to the PTH1R  $R^0$  conformation independent of G-protein coupling, whereas PTHrP binds with high affinity to the PTH1R  $R^G$  conformation, and the binding was dependent on G-protein coupling.<sup>24</sup> The two conformations also affect PTH1R function. The  $R^G$  conformation is more consistent with the classic GPCR ligand binding mechanisms and activation, while the  $R^0$  conformation stimulates sustained cAMP

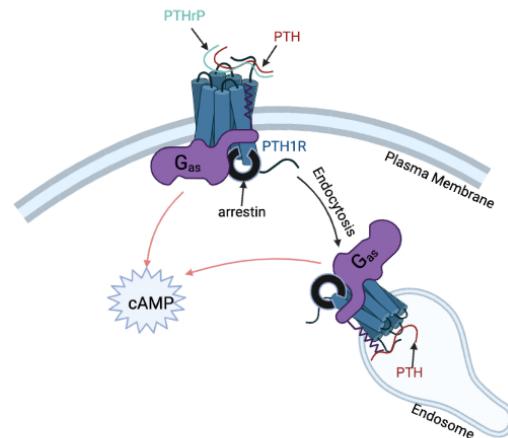


Figure 9: Canonical and noncanonical G-protein signaling at the PTH1R. PTHrP forms complexes with  $G_{\alpha s}$  and signals through cAMP only at the plasma membrane before dissociating, whereas PTH forms complexes both at the cell surface and remains associated as complexes internalize.

signaling through  $G_{\alpha s}$  pathway with prolonged PTH association with PTH1R. Because PTH remains bound to the  $R^0$  conformation of PTH1R, this complex continuously signals and induces the production of cAMP even after the internalization into the early endosome for degradation. Therefore, PTH1R can facilitate cAMP production both by the canonical mechanism operating at the surface of the plasma membrane through either the PTHrP-PTH1R/ $R^G$  complex or the PTH-PTH1R/ $R^0$  complex and by a noncanonical mechanism operating from the internalized endosomal domain via the PTH-PTH1R/ $R^0$  conformation (Figure 9).

Further studies utilizing fluorescence resonance energy transfer (FRET) based kinetics experiments showed PTH had a 66-fold greater binding capacity to the  $R^0$ , G-protein-uncoupled conformation. In similar experiments, PTHrP showed 16-fold higher selectivity for the  $R^G$  conformation than for  $R^0$  conformation when compared to PTH's conformational selectivity.<sup>31</sup> By utilizing FRET-based kinetics assays, the study also observed that PTH bound to PTH1R more rapidly and dissociated from the receptor more slowly than PTHrP. Further, the cAMP signaling response in cells stimulated by PTHrP binding decayed more rapidly than in PTH induced cAMP generation. Therefore, the PTH-bound  $R^0$  conformation produces cumulatively greater cAMP compared to PTHrP. More importantly, the study discovered that the divergent sequence at residue 5 in both hormones, isoleucine in PTH and histidine in PTHrP, is the major determinant for the conformational selectivity. A mutant PTH with histidine at residue 5 exhibited a decrease in binding affinity to  $R^0$  conformation, and a mutant PTHrP with isoleucine at residue 5 showed an increase in binding affinity to  $R^0$  conformation. The ability to swap conformational selectivity through a single hormone mutation is unique and highlights the importance of understanding how ligand binding affects PTH1R conformational dynamics.

Additional studies showed PTH selection for the  $R^0$  conformation leads to a more stable complex with PTH1R in  $R^0$  conformation, which produced more sustained cAMP responses intracellularly.<sup>32</sup> In addition, the study found that PTH analogs that couple to  $R^0$  conformation more selectively than PTH also form highly stable complexes with PTH1R and thereby facilitate sustained signaling responses in PTH1R-targeted bone and kidney cells. The responses included greater increase in trabecular bone volume and larger rise in cortical bone turnover in mice. Injecting mice with these more selective PTH analogs also induced a more prolonged increase in blood calcium and decrease in blood phosphate concentrations. The distinctive  $R^0$  and  $R^G$  conformations stimulated by different ligand binding not only further confirmed the role of PTH1R conformational dynamics but, more importantly, demonstrated that distinct conformations induce different intracellular and physiological changes. Careful study of PTH1R conformational dynamics will uncover more important conformational states while unveiling the significant physiological nuances associated with each conformation.

Under usual circumstances,  $\beta$ -arrestin couples to membrane-embedded GPCRs and tags the bound GPCRs for endocytosis to the endosome for degradation or recycling (Figure 2). However, inconsistent with conventional  $\beta$ -arrestin pathways, the interaction between PTH1R and  $\beta$ -arrestin can stimulate a  $G_s$ -mediated cAMP response.<sup>24</sup> The  $\beta$ -arrestin interactions with PTH1R in endosomes activate mitogen-activated protein (MAP) kinases, which phosphorylate and inhibit phosphodiesterase-4, an enzyme which is normally involved in GPCR degradation.

The inhibition of phosphodiesterase-4 in turn promotes long-lasting cAMP generation mediated by  $G_{\alpha s}$ . Moreover,  $\beta$ -arrestin stabilizes the PTH1R- $G_{\beta\gamma}$  assembly that leads to prolonged cAMP production. This stabilization happens when  $\beta$ -arrestin directly associates with a phosphorylated serine on the PTH1R C-terminal tail and indirectly interacts with PTH1R by binding to the  $G_{\beta\gamma}$ , which is also bound to the upstream portion of PTH1R C-terminal tail. The sustained cAMP signaling eventually terminates when the internalized vesicles containing PTH-PTH1R complexes mature through the endosomal pathway and come in contact with cargo-sorting retromer complex. The retromer complex is a peripheral membrane protein assembly that regulates sorting cargo proteins through the endosomal system and mediates retrograde flow to the trans-Golgi network. The PTH-PTH1R complex docks to the retromer sorting proteins during this endosomal trafficking process and disassociates from  $\beta$ -arrestin which eventually leads to signal termination. PTH1R likely undergoes conformational changes upon  $\beta$ -arrestin stabilization, which enables the receptor to exhibit unconventional termination process. Therefore, exploring the PTH1R conformational dynamics can decipher the mechanism of this distinctive termination signal that induces specific mechanisms of intracellular signaling.

Allosteric and other modulators regulate PTH1R conformational dynamics and signaling. Extracellular  $Ca^{2+}$  acts as a positive allosteric modulator of PTH1R and significantly changes the magnitude and kinetics of the sustained cAMP signaling response by prolonging ligand residence time and receptor activation.<sup>33</sup> Further, increased extracellular  $Ca^{2+}$  concentrations lead to faster recruitment of  $G_{\alpha s}$  protein, and the  $Ca^{2+}$  helps stabilize PTH-bound PTH1R in an active conformation, leading to an increase in the magnitude of PTH1R activation.<sup>33</sup> Additionally, PTH residue arginine (R) 25 and acidic residues on extracellular loop (ECL) 1 of PTH1R are the key determinants for endosomal cAMP signaling facilitated by PTH, likely by interacting with  $Ca^{2+}$  to stabilize the ligand interaction with PTH1R. The study observed that when the ECL1 acidic and negatively charged residues aspartates or glutamates were substituted with neutral serine at positions 251-254, 257, and 259, there was a decreased sensitivity to  $Ca^{2+}$  and the ECL1 mutants were unable to engage in sustained cAMP generation as efficiently as wild type (WT) PTH1R. However, a mutant PTH R25C (position 25 arginine to cysteine) revealed a complete loss of sensitivity to  $Ca^{2+}$  and a remarkably shorter cAMP production. The PTH R25C mutant was found in patients with severe hypocalcemia, despite normal levels of circulating ligand. Therefore, the decreased efficacy of PTH R25C mutant likely reduces PTH-induced cAMP signaling through the extracellular positive allosteric modulator  $Ca^{2+}$ .

Further,  $Ca^{2+}$  has been shown to be a positive allosteric modulator of PTH binding affinity to PTH1R in fluorescence anisotropy experiments.<sup>34</sup> In the presence of 15 mM extracellular  $Ca^{2+}$ , WT PTH exhibits a 5-fold higher binding affinity to PTH1R, indicating WT PTH senses the presence of extracellular  $Ca^{2+}$ . WT PTHrP did not show the sensitivity to the same concentration of  $Ca^{2+}$  as WT PTH. Because WT PTHrP showed the same binding affinity to PTH1R regardless of the presence or absence of  $Ca^{2+}$ , PTH(1-14)PTHrP(15-36), a chimeric hormone containing portions of PTH and PTHrP, was constructed which completely lacks the ability to sense  $Ca^{2+}$ . This suggests the C-terminal domain of PTH is necessary for the  $Ca^{2+}$

sensing ability. Furthermore, the study established that the negatively charged residues glutamate (E) at position 19 and 22 on PTH are the key determinates for PTH extracellular  $\text{Ca}^{2+}$  sensing ability. When negatively charged PTH residues E19 and E22 were substituted with nonpolar and neutral alanine, the sensitivity to  $\text{Ca}^{2+}$  from PTH was markedly reduced, as indicated by a decreased binding affinity of PTH mutant E19A E22A to PTH1R. Therefore, the study further supports the notion that both PTH and PTH1R are required for positive allosteric modulation of  $\text{Ca}^{2+}$ . Allosteric modulators like  $\text{Ca}^{2+}$  amplify the complexity of PTH1R conformational dynamics. To understand the distinctive intracellular responses and PTH1R functional dynamics associated with various conformational ensembles induced by allosteric modulators, it is crucial to resolve the receptor structures using advanced techniques, such as cryogenic Electron Microscopy (cryo-EM).

As discussed, previous studies of PTH1R ligand binding and activation have uncovered many likely receptor conformational states crucial for its function. More recent cryo-EM structures of PTH-PTH1R-  $\text{G}_s$  and PTHrP-PTH1R-  $\text{G}_s$  complexes further support the importance of PTH1R conformational dynamics and the crucial role of  $\text{Ca}^{2+}$  as a positive allosteric modulator.<sup>35</sup> There are many interesting interactions uncovered by these structures;

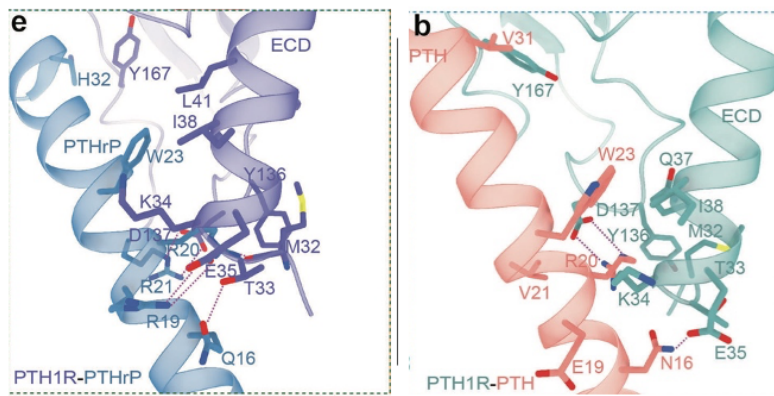


Figure 10 (Right): Molecular recognition of PTH1-34 (salmon) by PTH1R (green). Detailed interactions of PTH1R ECD with PTH C-terminus and PTH1R TMD pocket with PTH N-terminus can be seen. No polar interactions between PTH E19 with PTH1R. Figure 10 (Left): Molecular recognition of PTHrP1-36 (blue) by PTH1R (purple). Detailed interactions of PTH1R ECD with PTHrP C-terminus and PTH1R TMD pocket with PTHrP N-terminus. PTHrP R19 forming polar contacts with PTH1R (purple dotted lines).<sup>35</sup>

residues 19 and 22 are particularly relevant. First, both PTH and PTHrP show similar overall binding with the N-terminus binding in a pocket formed by PTH1R TMD and the C-terminus interacting with the PTH1R ECD. In the structure of PTH bound to PTH1R, residue E19 on PTH, which is potentially involved in  $\text{Ca}^{2+}$  modulation, showed no association with PTH1R (Figure 10 right).<sup>35</sup> In contrast, the structure of PTHrP bound PTH1R shows strong and important polar interactions between residue R19 of PTHrP

and E35 on PTH1R (Figure 10 left). The interactions between PTH1R and the distinct residues at position 19 on PTH and PTHrP suggests the difference in extracellular  $\text{Ca}^{2+}$  sensing ability of the two ligands might result from the different residues at position 19. Therefore, the distinctive interactions could potentially confirm the crucial role PTH E19 plays in extracellular  $\text{Ca}^{2+}$  sensing. On the other hand, a second cryo-EM study showed five distinctive conformations of PTH bound to PTH1R, while PTHrP bound PTH1R showed one active conformation.<sup>36</sup> The different structures of PTH1R show the potential for large changes in PTH1R conformational dynamics, especially when stimulated by PTH. We hypothesize that extracellular  $\text{Ca}^{2+}$  stabilizes the interaction between PTH and PTH1R, thus biasing PTH1R towards specific, long-lived,

activated conformations, which lead to more sustained intracellular downstream signaling. However, the specific interactions that lead to this stabilization are unknown. Understanding the mechanism of  $\text{Ca}^{2+}$  regulation will provide a clearer understanding of conformational dynamics in PTH1R, which is crucial for understanding the PTH1R physiological function.

It is necessary to understand the conformational dynamics of PTH1R because PTH1R plays a key role in the growth and development of skeletal tissue. Five loss-of-function mutations in PTH1R have been associated with certain diseases, including: osteochondrodysplasia, a rare but lethal condition defined by extremely advanced bone development; Ollier disease, a developmental condition characterized by occurrence of multiple enchondromas; Eiken syndrome, a rare recessive skeletal dysplasia resulted from severely delayed ossification; and Jansen's chondrodysplasia, a disorder that can lead to dwarfism and mineral ion imbalance.<sup>24</sup> Due to its vital role in bone remodeling, dysfunction of PTH1R has also been correlated with osteoporosis. Osteoporosis is a common bone disease which occurs when older bone breaks down but cannot be replaced by new bone. Bones can become brittle and weak due to osteoporosis, and even mild stresses such as coughing or bending down can result in bone fracture, leading to bone loss. The strongest risk factor for osteoporosis is a decrease in estrogen levels in women during menopause. However, other hormone changes can also lead to bone loss, such as overactive thyroid, parathyroid, and adrenal glands.<sup>37</sup> Currently, modified versions of the two hormones, PTH (1-34) and abaloparatide (ABL, PTHrP derivative), have been approved by the USFDA as treatments for severe osteoporosis, requiring daily subcutaneous injection. While these treatments increase bone density, their molecular mechanism is unclear.

In addition to osteoporosis, PTH can also be used to treat chronic hypothyroidism (HypoPT). HypoPT is characterized by an insufficient secretion of PTH accompanied by hypocalcemia (low blood calcium levels).<sup>38</sup> HypoPT is the most common complication following bilateral thyroid operations. Other risk factors of hypoPT include a substernal goiter, autoimmune thyroid disease, malabsorptive conditions, and central neck dissection. Conventional therapy for hypoPT aims to normalize calcium levels in serum. However, despite increased levels of serum calcium, patients with hypoPT often still suffer from a number of complications due to unbalanced physiological calcium-phosphate homeostasis.<sup>39</sup> Numerous studies recently have shown both full length PTH (1-84) and truncated PTH (1-34) have the capacity to normalize calcium levels in serum, reducing the need for vitamin D, magnesium, and calcium supplements in both children and adults either delivered through a continuous pump or twice daily injection.<sup>40,41</sup> However, while these treatments are effective, the role of PTH1R in the molecular mechanism of the treatments is poorly understood.

As mentioned above, PTH1R activates various signaling pathways. However, the mechanism by which PTH selectively activates distinct signaling pathways through PTH1R is still unknown. The current study aims to identify the signaling pathways mediated by specific  $G_\alpha$  isoforms that are activated by PTH and specifically understand if PTH selectively stimulates certain signaling pathways over the others due to changes in conformational dynamics. Understanding the connection between PTH activation of distinct signaling pathways through

PTH1R will shine a light on the role of PTH activation of PTH1R in metabolic bone remodeling, forming a foundation to develop more effective and accessible treatments for osteoporosis and hypothyroidism, such as oral hormone pills. Understanding G-protein selectivity and binding can also help to address other diseases involving PTH1R loss-of-function mutations and develop potential treatments to combat them.

Further, although recent studies revealed the role of extracellular  $\text{Ca}^{2+}$  as a positive allosteric modulator of PTH activation of PTH1R, the mechanism of the prolonged downstream signaling in the presence of extracellular  $\text{Ca}^{2+}$  is still puzzling. I hypothesize that the extracellular  $\text{Ca}^{2+}$  selectively modulates the conformational dynamics of PTH1R by stabilizing more active receptor conformations. The effect of the allosteric modulation of extracellular  $\text{Ca}^{2+}$  on the selection of specific G-protein-mediated signaling cascades is unknown and important, especially because PTH activates multiple signaling pathways via specific  $G_{\alpha}$  proteins coupling to PTH. Therefore, the goals of the current study are to identify changes in the interactions between G-protein isoforms and PTH1R in the presence and absence of extracellular  $\text{Ca}^{2+}$  when PTH1R is activated by either WTPTH or the PTHE19AE22A mutant.

Deciphering the mechanism of the effects of extracellular  $\text{Ca}^{2+}$  on different G-protein binding interactions will help us understand other long-term effects of hypoparathyroidism, hypocalcemia and other bone-related diseases. In this way, this work will uncover additional targets for specific signaling pathways associated with these diseases to combat downstream effects. For example, if the prolonged cAMP production in the presence of extracellular  $\text{Ca}^{2+}$  is due to tighter binding between PTH1R and  $G_{\alpha_s}$ , drug development could focus on a method to stabilize this interaction when extracellular  $\text{Ca}^{2+}$  is absent or in low concentration. More importantly, it has been shown PTH is able to activate the  $G_{\alpha_q}$  mediated signaling cascade which induces intracellular  $\text{Ca}^{2+}$  release as a downstream effect; a deeper connection between  $G_{\alpha_q}$  mediated signaling cascade and hypocalcemia can be further explored, and more methods to target hypocalcemia can be discovered in relation to the  $G_{\alpha_q}$  mediated signaling cascade.<sup>42</sup> Careful study of the mechanisms behind these crucial interactions in PTH1R will provide a strong foundation to better understand regulation of family-B GPCRs and their role in metabolic diseases.

### Experimental Approach

PTH1R activates multiple signaling pathways by coupling to the corresponding  $G_{\alpha}$  isoform, leading to distinct physiological effects. However, it is unclear if the observed differences in physiological effects are due to the ability of PTH to selectively activate distinct signaling pathways through PTH1R. Therefore,  $G_{\alpha}$  isoform selectivity of PTH upon activation of PTH1R will be explored utilizing Systematic Protein Affinity Strength modulation (SPASM) sensors. SPASM sensors will be used to measure the interactions between PTH-stimulated PTH1R and different isoforms of  $G_{\alpha}$ .<sup>43,44</sup> Two fluorophores, a donor and an acceptor, with different excitation and emission wavelengths will be attached to the C-terminal tail of the PTH1R. The fluorophores are connected by a flexible linker and then the desired  $G_{\alpha}$  peptide

( $G_{\alpha s}$ ,  $G_{\alpha i}$ ,  $G_{\alpha q}$ ) or No-peptide. Previous studies show the 27-residue  $G_{\alpha}$  peptide, which is the sequence of the  $\alpha 5$  helix, is sufficient to indicate interaction of a full  $G_{\alpha}$  subunit.<sup>45</sup> After specific excitation of the donor fluorophore, the emission of the donor fluorophore excites the acceptor fluorophore when the two are in close proximity (Figure 11). The ratio of acceptor emission to donor emission is measured as the FRET ratio, which indicates the distance between  $G_{\alpha}$  peptide and PTH1R. PTH will be added to cell membranes containing PTH1R-SPASM sensor linked with either  $G_s$ ,  $G_q$ ,  $G_i$  or No-peptide. The fluorophore emission counts at 525nm and 475nm will be measured, and the FRET ratio emission counts at 525nm and 475nm will be calculated. If there is a statistically significant increase in emitted fluorophore intensity after treatment with PTH compared to a buffer treatment condition, then PTH activates the specific linked  $G_{\alpha}$  protein and its corresponding signaling pathway.

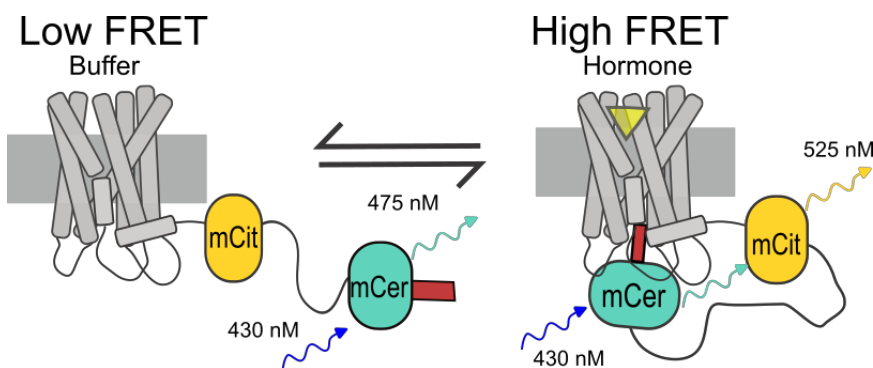


Figure 11: Schematics of the PTH1R C-terminal SPASM sensor (mCit-ER/K linker-mCer- $G_{\alpha}$ ) in the inactive (left) and active (right) conformation. mCit is the donor fluorophore, and mCer is the acceptor fluorophore.

To study SPASM sensors in fluorescence microscopy, the sensors need to be isolated from mammalian cells transiently transfected with SPASM sensors. Two methods to prepare SPASM sensors were explored. First, Giant Plasma Membrane Vesicles (GPMV) uses a GPMV buffer to vesiculate SPASM sensors embedded in the plasma membrane of the harvested cells. Then, GPMV containing SPASM sensors are isolated from other cells and debris through centrifugation (Figure 12).

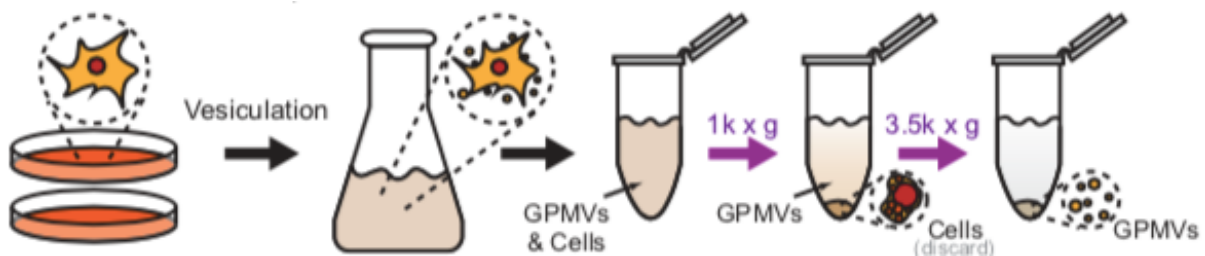


Figure 12: Workflow for preparing and isolating GPMVs.<sup>46</sup>

The second method involves preparations of native membranes from the mammalian cells. In this membrane preparation, after harvesting mammalian cells transiently transfected with SPASM sensors, the cells are lysed in a homogenizer. Then, multiple rounds of centrifugation

remove debris and cellular organelles. Membranes with the expressed SPASM sensors are pelleted through a final hard spin in an ultracentrifuge, resuspended, and flash frozen for future experimentation (Figure 13). Fluorescence data from both preparation mechanisms will be analyzed to determine the most effective method for studying PTH1R-G-protein interactions.



Figure 13: Membrane preparation workflow.

PTH1R-SPASM sensors will be used to determine how the  $\text{Ca}^{2+}$  modulation affects the specificity of G-protein coupling after PTH activation. The prolonged cAMP production in the presence of extracellular  $\text{Ca}^{2+}$  suggests changes in PTH1R activation of the  $G_{\alpha_s}$  mediated signaling pathway.<sup>33</sup> However, whether the prolonged signaling is due to changes in the interaction between PTH1R and  $G_{\alpha_s}$  is still unknown. Moreover, the effect of  $\text{Ca}^{2+}$  on other  $G_{\alpha}$  protein mediated signaling pathways is also unknown. The FRET ratio of PTH1R-SPASM sensors with  $G_s$ ,  $G_i$ ,  $G_q$  and a No-peptide control will be measured in the absence and presence of extracellular  $\text{Ca}^{2+}$ . Statistically significant changes in the FRET ratios after PTH activation in the presence of  $\text{Ca}^{2+}$  would indicate  $\text{Ca}^{2+}$  mediates more binding of the specific linked  $G_{\alpha}$  protein to PTH1R. Similar FRET assays will be performed with the PTHE19AE22A mutant, which showed partial abolishment of PTH  $\text{Ca}^{2+}$  sensing ability in  $G_{\alpha_s}$  mediated signaling pathways.<sup>34</sup> Changes in the FRET ratios after mutant PTHE19AE22A activation in the presence of extracellular  $\text{Ca}^{2+}$  would indicate reduced binding of the linked  $G_{\alpha}$  protein to PTH1R. Changes between the binding pattern of PTH and mutant PTHE19AE22A in the absence of extracellular  $\text{Ca}^{2+}$  will indicate the role of the PTH  $\text{Ca}^{2+}$  sensing ability in the selection of a specific  $G_{\alpha}$  corresponding signaling pathway.

### Significance

The combined results from these methods will enable us to identify the specific  $G_{\alpha}$  isoforms coupled to PTH1R and the associated pathways activated when stimulated by PTH. Understanding the selectivity of PTH to various  $G_{\alpha}$  isoforms can help develop more effective treatments for diseases involving PTH1R malfunctions where the abnormal downstream physiological effects are elicited by specific  $G_{\alpha}$  isoforms, which can then be specifically targeted.

The collective findings from PTH1R-SPASM sensors will reveal the relationship between extracellular  $\text{Ca}^{2+}$  and the binding affinity of PTH1R to various  $G_{\alpha}$  isoforms upon hormone activation. Studying PTH and the  $\text{Ca}^{2+}$  deficient mutant, PTHE19AE22A, will uncover the specificity of the hormone activation of G-protein isoforms and the impact of calcium

modulation. Understanding those relationships will decipher the mechanistic details about PTH1R activation and its role in bone related diseases, such as osteoporosis and hypocalcemia. Knowing the mechanistic characteristics of PTH1R and how they are regulated by extracellular  $\text{Ca}^{2+}$  can in turn establish a foundation for developing more effective and accessible drugs targeting known or novel bone related disease.

## Materials & Methods

**Reagents.** N-Ethylmaleimide (NEM, Tokyo chemical industry), synthesized WT PTH & PTHE19AE22A hormone (Biomatik), Fetal Bovine Serum (FBS, Avantor), HEK293T (ATCC, catalog number CRL-3216).

**DNA Constructs.** All constructs were expressed in the pcDNA5/FRT (ThermoFisher) vector. FRET-based SPASM sensor constructs used here contain, from N to C terminus, PTH1R, mCitrine (fluorescence acceptor), 10 nM ER/K  $\alpha$ -helix, mCerulean (fluorescence donor), and a 27 amino acid  $\text{G}\alpha$  C-terminal peptide.

**Cell culture.** HEK293T cells were cultured in Dulbecco's Modified Eagle Media (DMEM) containing 4.5 g/L D-glucose, with 10% FBS, 1% L-glutamine, and 20 mM HEPES, pH 7.5. Cells were maintained at 5%  $\text{CO}_2$  humidity at 37°C.

**Transient transfections.** For each GPMV purification, constructs described in current study were transiently transfected in HEK293T cells grown in 2 x 10 cm plate via an optimized protocol utilizing polyethylenimine (PEI, linear; molecular weight (MW), 25,000; PolySciences). For 2 x 10 cm plates, transfection mixture number one containing 40  $\mu\text{g}$  of the sensor DNA with 500  $\mu\text{L}$  of Opti-minimal essential medium media (Opt-MEM, Thermo Fisher) were mixed together, vortexed for 30-60 seconds, and incubated for 10 minutes at 25°C. Transfection mixture number two containing 100  $\mu\text{L}$  PEI with 500  $\mu\text{L}$  Opt-MEM were mixed together, vortexed for 30-60 seconds, and incubated for 10 minutes at 25°C. The two transfection mixtures were combined and mixed via gentle pipetting 10 times and incubated for another 3 minutes at 25°C before adding to the cells. The media with transfection reagents was exchanged with 10 mL fresh medium/plate after 2-3h of incubation at 37°C.

For each membrane preparation, constructs described in current study were transiently transfected in HEK293T cells grown in 2 x 15 cm plate via an optimized protocol utilizing polyethylenimine (PEI, linear; molecular weight (MW), 25,000; PolySciences). For 2 x 15 cm plates, transfection mixture number one containing 64  $\mu\text{g}$  of the sensor DNA with 1 mL of Opti-minimal essential medium media (Opt-MEM, Thermo Fisher) were mixed together, vortexed for 30-60 seconds, and incubated for 10 minutes at 25°C. Transfection mixture number two containing 200  $\mu\text{L}$  PEI with 1 mL Opt-MEM were mixed together, vortexed for 30-60 seconds, and incubated for 10 minutes at 25°C. The two transfection mixtures were combined and mixed via gentle pipetting 20 times and incubated for another 3 minutes at 25°C before adding to the cells. The media containing the transfection reagents were exchanged with 20 mL fresh medium after 2-3h of incubation at 37°C.

Expression and transfection efficiency was monitored with 20x and 40x magnification on a Nikon Eclipse Ts2-FL microscope equipped with fluorescence filter cubes.

**GPMV preparation and purification.** GPMVs were prepared as previously published from transfected HEK293T cells grown to at least 95% confluence expressing the desired PTH1R SPASM Sensor.<sup>46</sup> Cells were harvested and collected after 24h of expression time by pipetting in 10 mL tissue culture media and washed twice with phosphate buffered saline (PBS; 5 mL per 10 cm plate) before incubated in 10.8 mL of GPMV buffer for 2h at 30°C, shaking at 200 rpm in cell incubator. The GPMV buffer contains 10 mM Hepes pH 7.4, 150 mM NaCl, and 2 mM  $\text{CaCl}_2$ , 2 mM NEM, 2  $\mu\text{g}/\text{mL}$  PMSF. After vesiculation, cells and other debris were discarded through centrifugation, leaving the prepared GPMVs in the supernatant. GPMVs were centrifuged (3,220 x g, 40 min, 4°C), washed in 1 mL FRET

buffer (20 mM HEPES pH 7.4, 5 mM KCl, 145 mM NaCl, 2 mM CaCl<sub>2</sub> and 1 mM MgCl<sub>2</sub>) before being resuspended in 500  $\mu$ L FRET buffer. Prepared vesicles were stored on ice at 4° C and are stable for up to 1 month.

**Membrane preparations.** Membranes were prepared as previously published from transiently transfected HEK293T cells with 95% confluence expressing the desired PTH1R SPASM Sensor.<sup>46–48</sup> Cells were harvested and collected after 24h of expression time by scraping and pipetting in 20 mL tissue culture media then washed once with phosphate buffered saline (PBS; 5 mL per 15 cm plate). Pelleted cells were resuspended in 8 mL of chilled hypotonic buffer (10 mM HEPES, 50 mM EDTA, pH 7.4) with 5  $\mu$ g/ $\mu$ L PMSF. After 30 minutes incubation on ice, cells were gently lysed in a chilled dounce homogenizer (45 strokes) and crude membranes were separated from intact cells, nuclei, and debris by a low-speed spin (1,000  $\times$  g, 5 min, 4 °C). Membranes were harvested by ultracentrifugation at 150,000  $\times$  g, 30 min, 4 °C in a 70.1 TI rotor. Native membranes were resuspended in 1 mL FRET buffer with 12.5% sucrose (weight/volume) and homogenized, first by passing through a 26-gauge needle 5 times and then passing through a 20-gauge needle 5 times. SPASM Sensors were quantified using fluorescence emission scans (excitation 430 nm, emission scan 450 nm–600 nm) in a PTI Quantamaster 40 fluorescence spectrometer to confirm expression level and sensor integrity. Resuspended native membranes were aliquoted, flash frozen in liquid nitrogen, and stored at –80°C in FRET buffer with 12.5% sucrose.

**$\Delta$ FRET assay.** Native membranes from HEK293T cells transiently transfected with PTH1R-SPASM sensors were resuspended in FRET buffer based on mCerulean fluorescence ( $0.5 \times 10^6$  mCerulean counts at 475 nm). 1.5 mL of membrane solution was aliquoted into 10 tubes (135  $\mu$ L per tube). 5 tubes received 15  $\mu$ L 100  $\mu$ M agonist (PTH or PTHE19AE22A) treatment and 5 tubes received additional 15  $\mu$ L FRET buffer. Reactions were incubated for 5 min at 25°C shaking at 400 rpm after the addition of agonist or buffer. After 5 min of stimulation, 150  $\mu$ L of each reaction was transferred to an optical quartz cuvette (3-3.0-SOG-3, Starna Cells, Inc). Fluorescence spectra (PTI Quantamaster 40 fluorimeter) were measured for each sample (ex. 430 nm, em. 450 nm–600 nm). The mCitrine (emission 525 nm): mCerulean (emission 475 nm) ratio (FRET ratio) was calculated from each acquired spectrum. After background correction, the change in FRET ( $\Delta$ FRET) was determined by subtracting the average FRET ratio of the buffer conditions from the average of the agonist conditions.

**Data analysis.** Figures were generated and data statistical analysis were performed on Prism 9 using statistical tests indicated in preliminary data section.

## Preliminary Data

### SPASM Sensor preparation methods

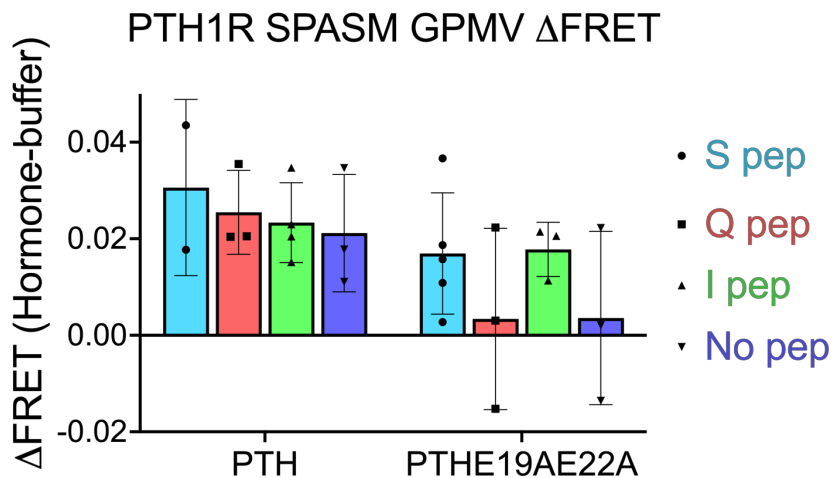


**Figure 14:  $\Delta$ FRET of GPMV SPASM sensors with WT PTH and PTHE19AE22A.**  $\Delta$ FRET of GPMV prepared SPASM sensors with each  $G_{\alpha}$  peptide. Treatments were WT PTH or mutant PTHE19AE22A, each compared to the buffer. Biological replicates are indicated by individual data points for each condition. Each biological replicate is the average of five technical replicates. Error bars represent one standard deviation.

SPASM sensors prepared in GPMVs from transiently transfected HEK293T cells were measured in FRET assays. An increase in  $\Delta$ FRET (hormone – buffer) was observed in the current study for PTH1R SPASM sensors with all peptides, including the No-peptide control, when PTH1R was activated by WT PTH compared to when PTH1R was at basal activation in the buffer condition. An increase in  $\Delta$ FRET was also

observed in the current study across all peptides when PTH1R was activated by the PTHE19AE22A mutant compared to when PTH1R was at basal activation in the buffer condition.  $\Delta$ FRET increases were lower in all peptides when PTH1R was activated by the PTHE19AE22A mutant compared to when PTH1R was activated by WT PTH, but a two-way ANOVA test with multi-comparison revealed the difference was not statistically significant. The  $\Delta$ FRET increases for PTH1R-SPASM sensors with S pep and I pep with PTHE19AE22A activation of PTH1R was more consistent compared to Q pep and No pep. However, a two-way ANOVA test with multi-comparison revealed the difference was not statistically significant. Due to the unexpected activation of No-peptide upon PTH binding to PTH1R, the current study investigated the effect of different preparation methods for SPASM sensors to optimize sensor signal and function.

To compare the effect of preparation method on fluorescence measures, fluorophore emission counts (475nm or 525nm) were compared to background emission (450nm) for PTH1R-SPASM sensors in native membrane preparations or GPMVs. SPASM sensors isolated through membrane preparations showed consistently higher fluorescent signals in both 525nm/450nm and 475nm/450nm across the buffer or WT PTH treatment than SPASM sensors isolated from GPMV method. SPASM sensors isolated through membrane preparations also generally showed less variability in the presence of either buffer or WT PTH condition compared to SPASM sensors prepared with the GPMV method, especially in the comparison of SPASM sensors 475nm/450nm in PTH treatment between membrane preparation and GPMV.

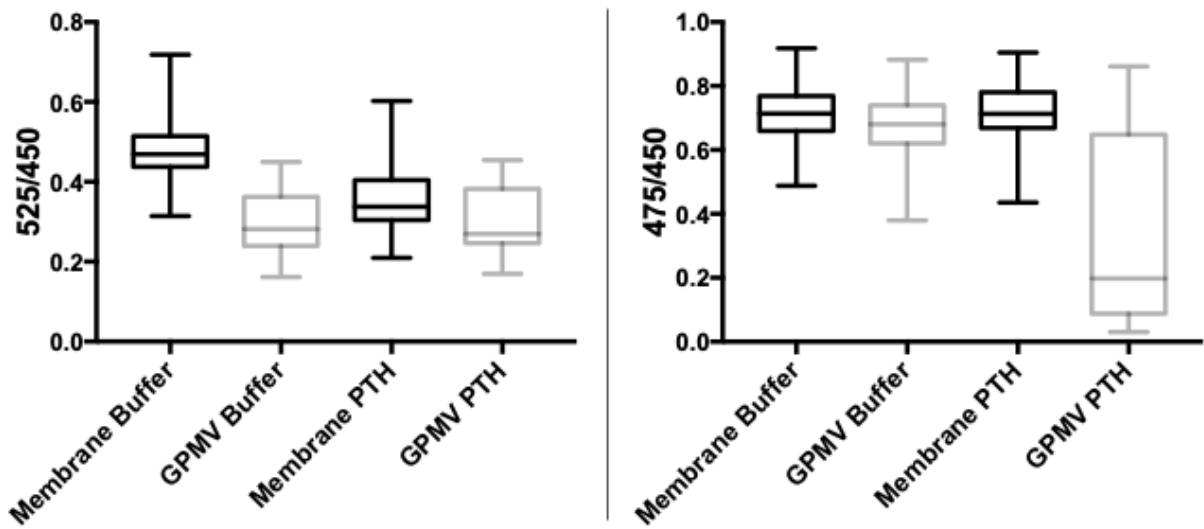


**Figure 15(Left): SPASM sensors 525nm/450nm fluorescent signal.** Box and Whisker plots showing SPASM sensors isolated through either membrane preparation (black) or GPMV method (light grey) in the presence of either buffer or WT PTH. **(Right): SPASM sensors 475nm/450nm fluorescent signal.** Box and Whisker plots showing SPASM sensors isolated through either membrane preparation (black) or GPMV method (light grey) in the presence of either buffer or WT PTH. (n=208 for membrane buffer, n=134 for membrane PTH, n=128 for GPMV buffer, n=60 for GPMV PTH)

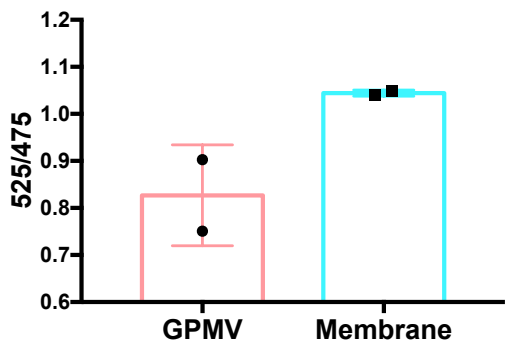


**Figure 16: SPASM sensors 525nm/475nm fluorescent signal.** SPASM sensors isolated through either membrane preparation (teal, n=342) or GPMV method (salmon, n=188) with combined 525nm/475nm WT PTH and buffer treatments. Error bars represent standard deviation.

In addition, the average FRET ratio for PTH1R-SPASM for each preparation method was compared. The SPASM sensors isolated through membrane preparation showed a higher FRET (525nm/475nm) signal of combined WT PTH and buffer treatments than the SPASM sensors (525nm/475nm) signal isolated with GPMV. The FRET (525nm/475nm) signal of SPASM sensors isolated through membrane preparation also showed less variability compared to the FRET (525nm/475nm) signal of SPASM sensors isolated with GPMV with combined PTH and buffer treatments.

The emission peaks for the donor (475nm) and acceptor (525nm) fluorophores are highly dependent on the background fluorescence from the preparation method (450nm). Untransfected cells were used as background controls for both GPMV and native membrane preparations. The fluorescence spectra of the untransfected cells were measured at multiple concentrations and subtracted from SPASM sensor preparations. SPASM sensors isolated through membrane preparation showed higher background-subtracted counts/second across wavelength at 450nm (background reference, no subtraction), 475nm, and 525nm than SPASM sensors isolated through GPMV background subtracted counts/second. GPMV background subtracted counts/second at wavelength 475nm and 525nm were close to or lower than zero. The data presented shows the background noise of the GPMV fluorescence obscures the signals from the PTH1R SPASM sensors.

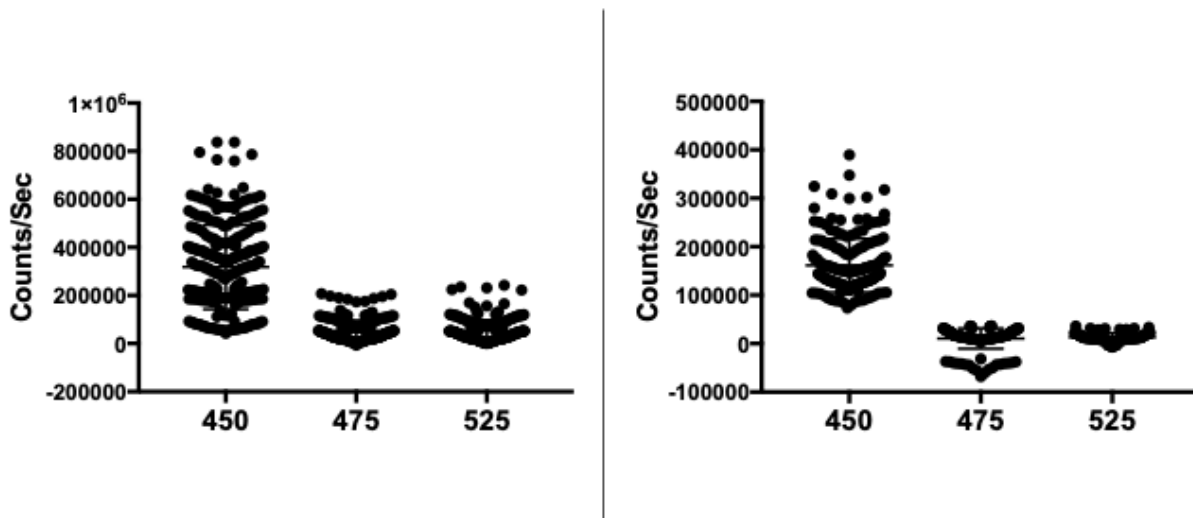


**Figure 17(Left):** SPASM sensors isolated through membrane preparation (n=342) counts/second at 450nm, 475nm, and 525nm with background subtracted. **(Right):** SPASM sensors isolated through GPMV (n=188) counts/second at 450nm, 475nm, and 525nm with background subtracted.

## PTH activates PTH1R-SPASM sensors

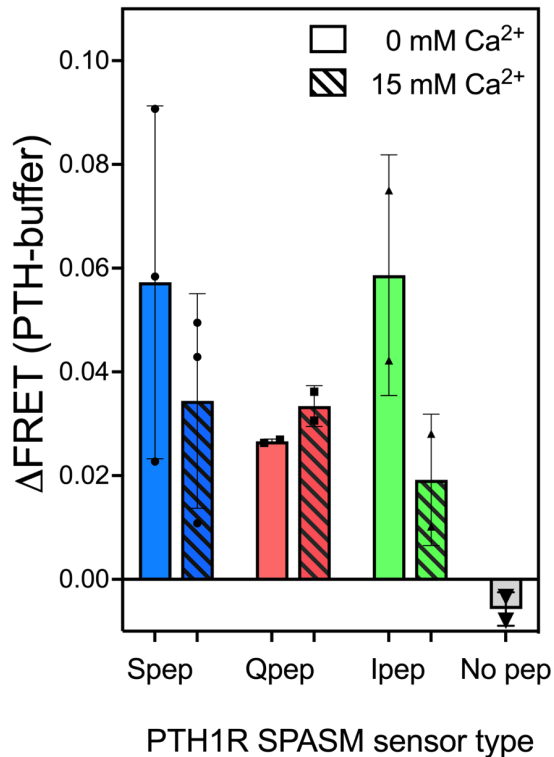


**Figure 18:  $\Delta$ FRET induced by WT PTH in the presence/absence of  $\text{Ca}^{2+}$ .** Different G peptides showed distinct interactions with PTH1R activated by PTH. The interactions were further altered by  $\text{Ca}^{2+}$ . Error bars represent one standard deviation.

increase in  $\Delta$ FRET in the presence of  $\text{Ca}^{2+}$  compared to the absence of  $\text{Ca}^{2+}$ . The data shows PTH1R-SPASM sensors detect changes in G-protein interactions for different G-protein peptides in the presence and absence of  $\text{Ca}^{2+}$ .

## Mutant PTHE19AE22A activates PTH1R-SPASM sensors

Membrane preparations of PTH1R-SPASM sensors were prepared from HEK283T cell transiently transfected with a PTH1R-SPASM sensor. The membranes were used to measure changes in FRET after PTH activation of PTH1R. Preliminary data shows an increase in  $\Delta$ FRET (PTH-buffer) in Spep, Qpep and Ipep sensors and no changes with the Nopep control sensors (Figure 18). The PTH1R-SPASM-Spep and Ipep sensors show a larger  $\Delta$ FRET in this preliminary data, but more biological replicates need to be collected to analyze the significance of the difference.

The addition of extracellular  $\text{Ca}^{2+}$  affected the measured  $\Delta$ FRET values in PTH1R-SPASM sensors. Specifically, the presence of  $\text{Ca}^{2+}$  decreased  $\Delta$ FRET in Spep and Ipep compared to  $\Delta$ FRET measured with no  $\text{Ca}^{2+}$ . The Ipep sensors showed a larger  $\Delta$ FRET decrease in the presence of  $\text{Ca}^{2+}$  than the Spep sensors, but more biological replicates need to be collected to analyze the significance of the difference. PTH1R-SPASM-Qpep sensors showed an

PTH activation of PTH1R-SPASM sensors leads to distinct interactions with G-peptide isoforms. PTH1R-SPASM sensors showed different G-peptide interaction profiles upon activation with PTHE19AE22A. An increase in  $\Delta$ FRET (PTHE19AE22A – buffer) for PTH1R-SPASM-Spep and Qpep occurred with PTHE19AE22A mutant activation (Figure 19). The  $\Delta$ FRET increase was greater for PTH1R-SPASM-Spep compared to Qpep, but more biological replicates need to be collected to analyze the significance of the difference. Further,  $\Delta$ FRET values upon PTH activation of PTH1R-SPASM sensors were greater than the  $\Delta$ FRET when PTH1R was activated by PTHE19AE22A, but more biological replicates need to be collected to analyze the significance of the difference. Of interest, negative  $\Delta$ FRET was observed when PTH1R-SPASM-Ipep sensors were activated by PTHE19AE22A, indicating that the Ipep interactions with PTH1R upon PTHE19AE22A activation decreased compared to interactions between Ipep and PTH1R under basal conditions of buffer.

The presence of  $\text{Ca}^{2+}$  affected the PTHE19AE22A activation of PTH1R-SPASM sensors. With the addition of  $\text{Ca}^{2+}$ , PTH1R-SPASM-Qpep sensors showed an increase in  $\Delta$ FRET. In contrast, the PTH1R-SPASM-Ipep sensors showed restored Ipep activation in the presence of  $\text{Ca}^{2+}$ . No data was collected for Spep during PTH1R activation by PTHE19AE22A in the presence of  $\text{Ca}^{2+}$ , and future experiments will work to replicate experimental data.

## Discussion

The G-protein selectivity of PTH1R has been previously studied through changes in downstream signaling pathways. However, the molecular mechanisms that govern specific interactions between different G-protein isoforms and PTH1R are unknown. The current study determined effective and feasible preparation mechanisms for PTH1R fluorescence sensors. These sensors were used to study the G-protein interaction profile of PTH1R after activation by different hormones under different  $\text{Ca}^{2+}$  conditions. While replication is required, preliminary data highlights the feasibility of the project and uncovers novel preliminary results.

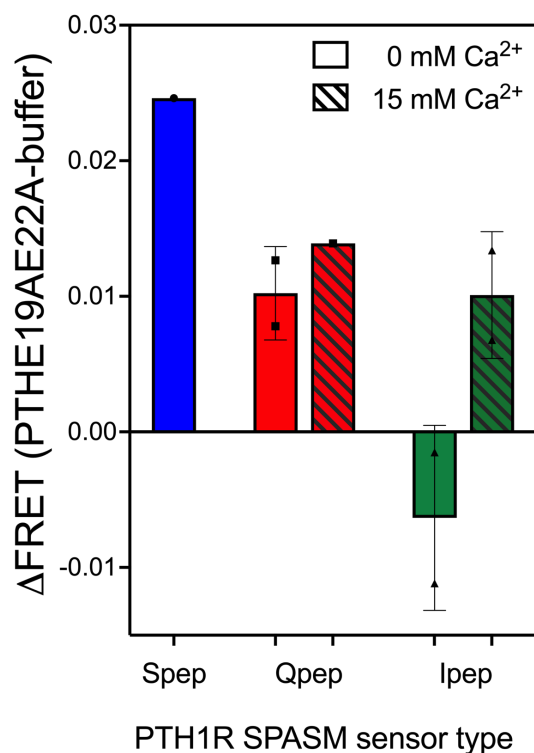


**Figure 19:  $\Delta$ FRET induced by PTHE19AE22A in the presence/absence of  $\text{Ca}^{2+}$ .** Different G peptides showed distinct interactions with PTH1R activated by PTH mutant. The interactions were further altered by  $\text{Ca}^{2+}$ . Error bars represent one standard deviation.

Initial studies measured changes in G-protein interactions using PTH1R-SPASM sensors prepared in GPMVs in fluorescence spectroscopy. However, the PTH1R-SPASM sensors with the No-peptide control prepared through the GPMV method showed increased  $\Delta$ FRET in the presence of both PTH and PTHE19AE22A (Figure 14). This result suggests that the scrambled No-peptide control sequence bound PTH1R activated by hormone binding. This is unexpected because interactions between PTH1R and G-proteins are sequence specific, meaning the scrambled sequence should not respond to hormone-stimulated PTH1R activation. Therefore, native membrane preparations were utilized to prepare SPASM sensors, and data was collected to compare the two preparation methods.

After measuring the non-specific binding in the PTH1R-SPASM-No-pep sensors prepared in GPMVs, the different fluorescence signals crucial for FRET were analyzed and compared for GPMVs and membranes. The following parameters were considered: background emission at 450nm, cerulean donor fluorophore emission peak at 475nm, and citrine acceptor fluorophore emission peak at 525nm. The PTH1R-SPASM sensors, isolated by membrane preparation, consistently showed higher ratios of donor and acceptor counts compared to the counts at 450nm, 475nm/450nm and 525nm/450nm, respectively, in both buffer and WT PTH treatments (Figure 15). These ratios are important because they indicate the signal level for each fluorophore, which depends on how well the cells express the SPASM sensor before preparation (the number of sensors), and the structural and functional integrity of the sensor (are both fluorophores attached and present). These results indicate SPASM sensors, isolated by membrane preparation, have higher expression level and better sensor integrity, respectively.

The next important metric is the emission of each fluorophore in counts per second after subtracting the background contributions. In this case, SPASM sensors in prepared membranes also showed higher counts per second with background subtraction at the citrine emission wavelength of 525nm and cerulean emission wavelength of 475nm (Figure 16). The counts per second at those two measured emission wavelengths of SPASM sensors prepared by GPMV were almost undetectable. Therefore, GPMV isolated SPASM sensors did not have high enough fluorescent signals and were not functional enough to conduct experiments. In addition, the individual data points of membrane prepared SPASM sensors were more consistent than the individual data points of GPMV isolated SPASM sensors, indicating more reliable results. Finally, the FRET ratios (525nm/475nm) of SPASM sensors isolated through membrane preparation were higher, which is expected based on previous studies of the GPCRs in SPASM sensors, and less variable.<sup>43</sup> Therefore, membranes prepared through membrane preparation would be more suitable and dependable for  $\Delta$ FRET assay.

After determining the membrane preparation protocol was the most effective for fluorescence assays, the PTH1R-SPASM sensors were used to determine changes in FRET under different interacting conditions. Preliminary data of SPASM sensors in prepared membranes showed an increase in  $\Delta$ FRET in the presence of WT PTH across all G-peptide isoforms, with no change for the No-peptide control. These results suggest that WT PTH activates PTH1R interactions with  $G_{\alpha s}$ ,  $G_{\alpha i}$ ,  $G_{\alpha q}$  isoforms. A stronger  $\Delta$ FRET increase was observed in PTH1R-SPASM-Spep and Ipep, indicating PTH1R preferentially interacts more with  $G_{\alpha s}$  and  $G_{\alpha i}$ . Further, the presence of 15 mM  $Ca^{2+}$  modulates the interactions of PTH1R-SPASM sensors for all peptides.

The decrease in  $\Delta$ FRET in Spep and Ipep and the increase in  $\Delta$ FRET in Qpep when 15mM  $\text{Ca}^{2+}$  was added with WT PTH indicated PTH1R interacts less through  $G_{\alpha_s}$  and  $G_{\alpha_i}$  pathways and more with  $G_{\alpha_q}$  pathways when activated by WT PTH in the presence of  $\text{Ca}^{2+}$ . However, additional  $\Delta$ FRET assays with more biological replicates need to be conducted before any significant conclusion can be drawn.

The PTH1R-SPASM sensors showed distinct G-protein interactions after activation by the mutant hormone PTHE19AE22A. Preliminary data from prepared membranes with PTH1R-SPASM sensors showed increases in Spep and Qpep  $\Delta$ FRET, with a decrease in Ipep  $\Delta$ FRET after activation by PTHE19AE22A. These results suggest PTH1R was able to signal through  $G_{\alpha_s}$  and  $G_{\alpha_q}$  signaling pathways upon PTHE19AE22A activation. A larger  $\Delta$ FRET increase was observed in PTH1R-SPASM-Spep compared to the Qpep sensors, indicating increased PTH1R activation of  $G_{\alpha_s}$  upon PTHE19AE22A binding. In contrast, PTHE19AE22A binding to PTH1R-SPASM sensors did not favor  $G_{\alpha_i}$  activation because the measured  $\Delta$ FRET was negative. PTHE19AE22A caused the Ipep to bind PTH1R-SPASM sensor less than the buffer basal conditions, suggesting PTHE19AE22A shuts down  $G_{\alpha_i}$  interactions with PTH1R. The presence of 15mM  $\text{Ca}^{2+}$  restored PTH1R interactions with  $G_{\alpha_i}$ , which indicates the presence of  $\text{Ca}^{2+}$  likely induces a conformational change in PTH1R that allosterically allows  $G_{\alpha_i}$  interaction even with PTHE19AE22A bound. Finally, the increase in  $\Delta$ FRET in PTH1R-SPASM-Qpep when 15mM  $\text{Ca}^{2+}$  was added with PTHE19AE22A indicated PTH1R signals more through  $G_{\alpha_q}$  pathways when activated by PTHE19AE22A in the presence of  $\text{Ca}^{2+}$ . However, additional  $\Delta$ FRET assays with more biological replicates need to be conducted before determining the significance of the results.

The results from the PTH1R-SPASM sensors begin to outline possible relationships in how ligand and G-protein binding affect PTH1R conformational dynamics and selection of distinct signaling pathways. These data fit with the knowledge in the field that GPCRs are extremely complex conformationally. GPCRs undergo numerous transient structural changes upon ligand, G-protein, or nucleotide binding. The various structural conformations often indicate differential activation levels in receptors which therefore elicit distinctive types or strengths of downstream signaling, leading to various cellular or physiological responses. For example, a recent study utilized cryo-EM to visualize 20 distinctive reconstructions of  $\beta_2$ -AR in complex with the heteromeric  $G_s$  protein at short sequential time points.<sup>49</sup> Structures were solved after GTP addition during the trajectory of G-protein coupling and showed GDP release, GTP activation of G-protein heterotrimer, and G-protein heterotrimer functional dissociation from a GPCR. While the functional states in  $\beta_2$ -AR are well studied, PTH1R shows similar, but unique, structural complexity. As mentioned above, a recent cryo-EM study of a PTH-PTH1R- $G_s$  complex revealed five distinct conformations of PTH1R upon PTH binding.<sup>36</sup> Different structures indicate multiple potential conformations of PTH1R, each of which might activate different intracellular downstream signaling pathways and serve distinctive biological functions.

Recent work shows the conformational dynamics for a given GPCRs are dictated by certain receptor domains. One such domain is ICL3, the largest of the three intracellular loops, which plays a major role in family-A GPCRs activation of downstream signal transduction processes. ICL3 connects transmembrane helices 5 and 6 that regulate receptor activation and inactivation through major conformational changes.<sup>50</sup> A recently published study found that  $\beta_2$ -

AR selectivity for G-protein subtypes was achieved via a dynamic conformational equilibrium that enables ICL3 to autoregulate  $\beta$ 2-AR activation by blocking or exposing the G-protein binding site.<sup>48</sup> Thus, this gating mechanism prevents the receptor from interacting with G-protein subtypes that normally only weakly couple to the GPCR. Furthermore, the study demonstrated that the ICL3-gated, negative G-protein-selection mechanism was shared among GPCR superfamilies and dependent on ICL3 length. When the  $\beta$ 2-AR ICL3 was grafted into PTH1R, the study observed an increase in cAMP  $E_{max}$  ( $G_s$  signaling) and a decrease in  $InsP_1 E_{max}$  ( $G_q$  signaling) in the chimeric receptor, PTH1R- $\beta$ 2-ARICL3. This is significant because WT PTH1R has a short ICL3 and couples primarily to  $G_{\alpha_s}$  and secondarily to  $G_{\alpha_q}$ . By altering the length and sequence of ICL3, PTH1R was tailored to signal through  $G_{\alpha_q}$  rather than  $G_{\alpha_s}$  thus changing PTH1R G-protein subtype specificity.

In addition to dictating the G-protein subtype selectivity for GPCRs, ICL3 also harbors conserved binding sites for allosteric modulators such as the sodium ion ( $Na^+$ ). For example, one study confirmed that  $Na^+$  in physiological concentration serves as a negative allosteric modulator for the agonist [ $^3H$ ]NECA binding to  $A_{2A}AR$ .<sup>11</sup> The modulation occurs through the interaction with a highly conserved residue Asp52 and coordination between Ser91 and three water molecules in the  $A_{2A}AR$  TM7 bundle. It has also been known that the allosteric binding site on  $A_{2A}AR$  ICL3 is shared between  $Na^+$  and amiloride. One study demonstrated that while amiloride and its analogues accelerated the dissociation of antagonist [(3)H]ZM241385,  $Na^+$ , decreased the rate of the antagonist dissociation in a concentration-dependent manner.<sup>51</sup> Therefore, the competition between amiloride and  $Na^+$  for the allosteric binding site on  $A_{2A}AR$  ICL3 mediates the receptor activity.  $Na^+$  likely regulates  $A_{2A}AR$  activation by acting as different modulators for antagonist and agonist through the association with highly conserved residues on ICL3.

Similar flexible domains on PTH1R are likely regulated by extracellular  $Ca^{2+}$ . The specific domain that likely dictates PTH1R activation states is ECL1, which harbors a potential allosteric binding site for  $Ca^{2+}$  and participates

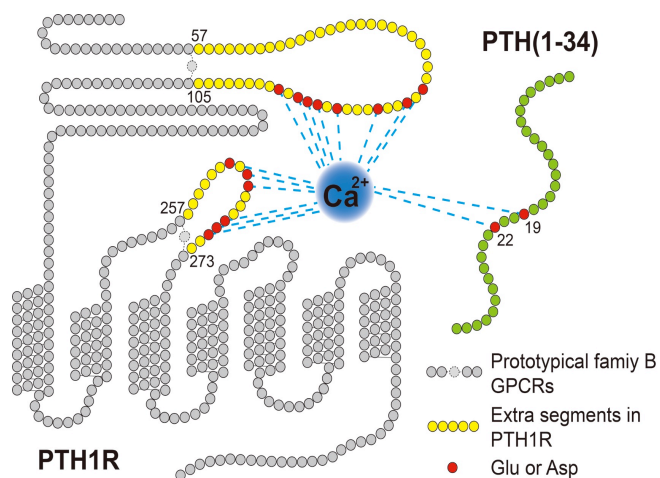


Figure 20: Snake plot of PTH1R and PTH showing negatively charged residues in red, which are clustered towards the extracellular side of the receptor. Two regions of PTH1R not conserved in family B GPCRs are colored: the 50-residue flexible loop in ECD contains 8 negatively charged residues and the 16-residue ECL1 contains 6 negatively charged residues.

in  $Ca^{2+}$  sensing. As mentioned earlier in this study, a chimeric hormone comprised of PTH N-terminal domain and PTHrP C-terminal domain exhibit no  $Ca^{2+}$  sensitivity but mutant hormone PTH(1-34)E22A only showed a partial decrease in  $Ca^{2+}$  sensing ability.<sup>34</sup> Therefore, the study suggested PTH1R, along with PTH, both contribute to  $Ca^{2+}$  sensing. The study proposed that the ECD flexible loop and ECL1, containing many negatively charged residues, are the two regions of the receptor that are specifically responsible for  $Ca^{2+}$  sensitivity (Figure 20). Further, as discussed earlier in this study, White

et al., (2019) identified that the negatively charged residues on PTH1R ECL1 are the major determinates for  $\text{Ca}^{2+}$  sensitivity and PTH stabilization.<sup>33</sup> By replacing negatively charged residues in PTH1R ECL1 with neutral serine at multiple positions, the study observed a reduction sensitivity to  $\text{Ca}^{2+}$  and a loss of ability to maintain prolonged downstream signaling for cAMP production.

The current study examined the role of two acidic residues in hormone PTH in  $\text{Ca}^{2+}$  sensitivity, but as demonstrated in numerous previous studies, PTH1R  $\text{Ca}^{2+}$  sensing ability is achieved through the collaboration between both PTH and the receptor itself. In addition to the required replication of the preliminary data presented here, further research will aim to explore the importance of receptor acidic residues in  $\text{Ca}^{2+}$  sensitivity, especially those on ECL1. The negatively charged residues in PTH1R might assist  $\text{Ca}^{2+}$  to stabilize PTH and thus establish higher binding affinity between the hormone and the receptor. I hypothesize that the flexibility of ECL1 enables PTH1R to achieve the distinct active states previously observed through cryo-EM. The presence of negatively charged residues on ECL1 allow  $\text{Ca}^{2+}$  to stabilize specific states when PTH is bound, which induces alterations to PTH1R conformational dynamics. Thus, a specific, stabilized conformation of ECL1 is required for the selection of the most active states of PTH1R.

Understanding the specific and distinctive PTH1R signaling pathways induced by either PTH or PTH19AE22A while uncovering  $\text{Ca}^{2+}$  modulation in these various signaling pathways is crucial, since abnormal regulation of PTH1R and mutations in PTH have been shown to be associated with numerous diseases such as hypocalcemia, hypothyroidism, and osteoporosis. More importantly, agonists of PTH have been shown to effectively treat hypothyroidism and osteoporosis. Therefore, delineating the mechanistic details of PTH1R activation by PTH and their relation to bone-related diseases will help develop more efficient and accessible treatments that specifically target certain diseases, while unveiling the specific role of PTH1R in bone remodeling. Most encouragingly, the FRET-based SPASM sensors equipped us with the ability to examine the finer PTH1R activation mechanistic details, providing the foundation to better understand these crucial molecular interactions.

### **Acknowledgment**

Special gratitude to Dr. Kelly Culhane for experimental support and guidance along with current thesis suggestions and modifications. Special thanks to Iris Cobb & Midushi Ghimire for project collaboration. Special thanks Maheen Iftikha, Kaia Houtman, Adriana Hudyma, & Alexa Burton for lab assistance. Special thanks to Itai S. Bojdak-Yates & Ryan Knepel for proofreading.

### **Citations**

- (1) Manglik, A.; Kobilka, B. K.; Steyaert, J. Nanobodies to Study G Protein-Coupled Receptor Structure and Function. *Annu Rev Pharmacol Toxicol* **2017**, *57*, 19–37. <https://doi.org/10.1146/annurev-pharmtox-010716-104710>.
- (2) Hauser, A. S.; Attwood, M. M.; Rask-Andersen, M.; Schiöth, H. B.; Gloriam, D. E. Trends in GPCR Drug Discovery: New Agents, Targets and Indications. *Nat Rev Drug Discov* **2017**, *16* (12), 829–842. <https://doi.org/10.1038/nrd.2017.178>.

- (3) Hauser, A. S.; Chavali, S.; Masuho, I.; Jahn, L. J.; Martemyanov, K. A.; Gloriam, D. E.; Babu, M. M. Pharmacogenomics of GPCR Drug Targets. *Cell* **2018**, *172* (1–2), 41–54.e19. <https://doi.org/10.1016/j.cell.2017.11.033>.
- (4) Inoue, A.; Raimondi, F.; Kadji, F. M. N.; Singh, G.; Kishi, T.; Uwamizu, A.; Ono, Y.; Shinjo, Y.; Ishida, S.; Arang, N.; Kawakami, K.; Gutkind, J. S.; Aoki, J.; Russell, R. B. Illuminating G-Protein-Coupling Selectivity of GPCRs. *Cell* **2019**, *177* (7), 1933–1947.e25. <https://doi.org/10.1016/j.cell.2019.04.044>.
- (5) Devree, B. T.; Mahoney, J. P.; Vélez-Ruiz, G. A.; Rasmussen, S. G. F.; Kuszak, A. J.; Edwald, E.; Fung, J. J.; Manglik, A.; Masureel, M.; Du, Y.; Matt, R. A.; Pardon, E.; Steyaert, J.; Kobilka, B. K.; Sunahara, R. K. Allosteric Coupling from G Protein to the Agonist-Binding Pocket in GPCRs. *Nature* **2016**, *535* (7610), 182–186. <https://doi.org/10.1038/nature18324>.
- (6) Chachisvilis, M.; Zhang, Y.-L.; Frangos, J. A. *G Protein-Coupled Receptors Sense Fluid Shear Stress in Endothelial Cells*; 2006. [www.pnas.org/cgi/doi/10.1073/pnas.0607224103](http://www.pnas.org/cgi/doi/10.1073/pnas.0607224103).
- (7) Dawaliby, R.; Trubbia, C.; Delporte, C.; Masureel, M.; Van Antwerpen, P.; Kobilka, B. K.; Govaerts, C. Allosteric Regulation of G Protein-Coupled Receptor Activity by Phospholipids. *Nat Chem Biol* **2016**, *12* (1), 35–39. <https://doi.org/10.1038/nchembio.1960>.
- (8) Oates, J.; Watts, A. Uncovering the Intimate Relationship between Lipids, Cholesterol and GPCR Activation. *Current Opinion in Structural Biology*. December 2011, pp 802–807. <https://doi.org/10.1016/j.sbi.2011.09.007>.
- (9) Mahaut-Smith, M. P.; Martinez-Pinna, J.; Gurung, I. S. A Role for Membrane Potential in Regulating GPCRs? *Trends Pharmacol Sci* **2008**, *29* (8), 421–429. <https://doi.org/10.1016/J.TIPS.2008.05.007>.
- (10) Ghanouni, P.; Schambye, H.; Seifert, R.; Lee, T. W.; Rasmussen, S. G. F.; Gether, U.; Kobilka, B. K. The Effect of PH on B2 Adrenoceptor Function. Evidence for Protonation-Dependent Activation. *Journal of Biological Chemistry* **2000**, *275* (5), 3121–3127. <https://doi.org/10.1074/jbc.275.5.3121>.
- (11) Liu, W.; Chun, E.; Thompson, A. A.; Chubukov, P.; Xu, F.; Katritch, V.; Han, G. W.; Roth, C. B.; Heitman, L. H.; IJzerman, A. P.; Cherezov, V.; Stevens, R. C. Structural Basis for Allosteric Regulation of GPCRS by Sodium Ions. *Science (1979)* **2012**, *337* (6091), 232–236. <https://doi.org/10.1126/science.1219218>.
- (12) Lander, G. H.; Emery, V. J. Diversity of G Proteins in Signal Trasnduction. *Nucl Instrum Methods Phys Res B* **1985**, *12* (4), 525–561. [https://doi.org/10.1016/0168-583x\(85\)90510-5](https://doi.org/10.1016/0168-583x(85)90510-5).
- (13) Shen, J. X.; Cooper, D. M. F. AKAP79, PKC, PKA and PDE4 Participate in a Gq-Linked Muscarinic Receptor and Adenylate Cyclase 2 CAMP Signalling Complex. *Biochemical Journal* **2013**, *455* (1), 47–56. <https://doi.org/10.1042/BJ20130359>.
- (14) Kozasa, T.; Hajicek, N.; Chow, C. R.; Suzuki, N. Signalling Mechanisms of RhoGTPase Regulation by the Heterotrimeric G Proteins G12 and G13. *J Biochem* **2011**, *150* (4), 357–369. <https://doi.org/10.1093/jb/mvr105>.
- (15) Zhang, X.; Kim, K. M. Multifactorial Regulation of g Protein-Coupled Receptor Endocytosis. *Biomol Ther (Seoul)* **2017**, *25* (1), 26–43. <https://doi.org/10.4062/biomolther.2016.186>.

- (16) Luttrell, L. M.; Lefkowitz, R. J. The Role of  $\beta$ -Arrestins in the Termination and Transduction of G-Protein-Coupled Receptor Signals. *J Cell Sci* **2002**, *115* (3), 455–465. <https://doi.org/10.1242/jcs.115.3.455>.
- (17) De Lean, A.; Stadel, J. M.; Lefkowitz, R. J. A Ternary Complex Model Explains the Agonist-Specific Binding Properties of the Adenylate Cyclase-Coupled  $\beta$ -Adrenergic Receptor. *Journal of Biological Chemistry* **1980**, *255* (15), 7108–7117. [https://doi.org/10.1016/s0021-9258\(20\)79672-9](https://doi.org/10.1016/s0021-9258(20)79672-9).
- (18) Dror, R. O.; Arlow, D. H.; Maragakis, P.; Mildorf, T. J.; Pan, A. C.; Xu, H.; Borhani, D. W.; Shaw, D. E.; Research, D. E. S.; York, N.; Levitt, M. Activation Mechanism of the  $\beta$  2-Adrenergic Receptor. <https://doi.org/10.1073/pnas.1110499108/-/DCSupplemental>.
- (19) Nygaard, R.; Zou, Y.; Dror, R. O.; Mildorf, T. J.; Arlow, D. H.; Manglik, A.; Pan, A. C.; Liu, C. W.; Fung, J. J.; Bokoch, M. P.; Thian, F. S.; Kobilka, T. S.; Shaw, D. E.; Mueller, L.; Prosser, R. S.; Kobilka, B. K. The Dynamic Process of B2-Adrenergic Receptor Activation. *Cell* **2013**, *152* (3), 532–542. <https://doi.org/10.1016/j.cell.2013.01.008>.
- (20) Bockenhauer, S.; Fürstenberg, A.; Yao, X. J.; Kobilka, B. K.; Moerner, W. E. Conformational Dynamics of Single G Protein-Coupled Receptors in Solution. *Journal of Physical Chemistry B* **2011**, *115* (45), 13328–13338. <https://doi.org/10.1021/jp204843r>.
- (21) Lamichhane, R.; Liu, J. J.; Pljevaljcic, G.; White, K. L.; Van Schans, E. Der; Katritch, V.; Stevens, R. C.; Wüthrich, K.; Millar, D. P. Single-Molecule View of Basal Activity and Activation Mechanisms of the G Protein-Coupled Receptor B2 AR. *Proc Natl Acad Sci U S A* **2015**, *112* (46), 14254–14259. <https://doi.org/10.1073/pnas.1519626112>.
- (22) Manglik, A.; Kim, T. H.; Masureel, M.; Altenbach, C.; Yang, Z.; Hilger, D.; Lerch, M. T.; Kobilka, T. S.; Thian, F. S.; Hubbell, W. L.; Prosser, R. S.; Kobilka, B. K. Structural Insights into the Dynamic Process of B2-Adrenergic Receptor Signaling. *Cell* **2015**, *161* (5), 1101–1111. <https://doi.org/10.1016/j.cell.2015.04.043>.
- (23) Gregorio, G. G.; Masureel, M.; Hilger, D.; Terry, D. S.; Juette, M.; Zhao, H.; Zhou, Z.; Perez-Aguilar, J. M.; Hauge, M.; Mathiasen, S.; Javitch, J. A.; Weinstein, H.; Kobilka, B. K.; Blanchard, S. C. Single-Molecule Analysis of Ligand Efficacy in B2AR-G-Protein Activation. *Nature* **2017**, *547* (7661), 68–73. <https://doi.org/10.1038/nature22354>.
- (24) Gardella, T. J.; Vilardaga, J. P. International Union of Basic and Clinical Pharmacology. XCIII. the Parathyroid Hormone Receptors—Family B G Protein–Coupled Receptors. *Pharmacol Rev* **2015**, *67* (2), 310–337. <https://doi.org/10.1124/pr.114.009464>.
- (25) Dong, S.; Shang, S.; Li, J.; Tan, Z.; Dean, T.; Maeda, A.; Gardella, T. J.; Danishefsky, S. J. Engineering of Therapeutic Polypeptides through Chemical Synthesis: Early Lessons from Human Parathyroid Hormone and Analogues. *J Am Chem Soc* **2012**, *134* (36), 15122–15129. <https://doi.org/10.1021/ja306637u>.
- (26) Li, J.; Dong, S.; Townsend, S. D.; Dean, T.; Gardella, T. J.; Danishefsky, S. J. Chemistry as an Expanding Resource in Protein Science: Fully Synthetic and Fully Active Human Parathyroid Hormone-Related Protein (1 - 141). *Angewandte Chemie - International Edition* **2012**, *51* (49), 12263–12267. <https://doi.org/10.1002/anie.201207603>.
- (27) Sutkeviciute, I.; Clark, L. J.; White, A. D.; Gardella, T. J.; Vilardaga, J. P. PTH/PTHrP Receptor Signaling, Allostery, and Structures. *Trends in Endocrinology and Metabolism* **2019**, *30* (11), 860–874. <https://doi.org/10.1016/j.tem.2019.07.011>.
- (28) Singh, A. T. K.; Gilchrist, A.; Voyno-Yasenetskaya, T.; Radeff-Huang, J. M.; Stern, P. H.  $G\alpha_{12}/G\alpha_{13}$  Subunits of Heterotrimeric G Proteins Mediate Parathyroid Hormone

- Activation of Phospholipase D in UMR-106 Osteoblastic Cells. *Endocrinology* **2005**, *146* (5), 2171–2175. <https://doi.org/10.1210/en.2004-1283>.
- (29) Iida-Klein, A.; Guo, J.; Takemura, M.; Drake, M. T.; Potts, J. T.; Abou-Samra, A.; Bringham, F. R.; Segre, G. V. Mutations in the Second Cytoplasmic Loop of the Rat Parathyroid Hormone (PTH)/PTH-Related Protein Receptor Result in Selective Loss of PTH-Stimulated Phospholipase C Activity. *Journal of Biological Chemistry* **1997**, *272* (11), 6882–6889. <https://doi.org/10.1074/jbc.272.11.6882>.
- (30) Huang, Z.; Chen, Y.; Pratt, S.; Chen, T. H.; Bambino, T.; Nissenson, R. A.; Shoback, D. M. The N-Terminal Region of the Third Intracellular Loop of the Parathyroid Hormone (PTH)/PTH-Related Peptide Receptor Is Critical for Coupling to CAMP and Inositol Phosphate/Ca<sup>2+</sup> Signal Transduction Pathways. *Journal of Biological Chemistry* **1996**, *271* (52), 33382–33389. <https://doi.org/10.1074/jbc.271.52.33382>.
- (31) Dean, T.; Vilardaga, J. P.; Potts, J. T.; Gardella, T. J. Altered Selectivity of Parathyroid Hormone (PTH) and PTH-Related Protein (PTHrP) for Distinct Conformations of the PTH/PTHrP Receptor. *Molecular Endocrinology* **2008**, *22* (1), 156–166. <https://doi.org/10.1210/me.2007-0274>.
- (32) Okazaki, M.; Ferrandon, S.; Vilardaga, J. P.; Bouxsein, M. L.; Potts, J. T.; Gardella, T. J. Prolonged Signaling at the Parathyroid Hormone Receptor by Peptide Ligands Targeted to a Specific Receptor Conformation. *Proc Natl Acad Sci U S A* **2008**, *105* (43), 16525–16530. <https://doi.org/10.1073/pnas.0808750105>.
- (33) White, A. D.; Fang, F.; Jean-Alphonse, F. G.; Clark, L. J.; An, H. J.; Liu, H.; Zhao, Y.; Reynolds, S. L.; Lee, S.; Xiao, K.; Sutkeviciute, I.; Vilardaga, J. P. Ca<sup>2+</sup> Allosterism in PTH-Receptor Signaling. *Proc Natl Acad Sci U S A* **2019**, *116* (8), 3294–3299. <https://doi.org/10.1073/pnas.1814670116>.
- (34) Culhane, K. J.; Belina, M. E.; Sims, J. N.; Cai, Y.; Liu, Y.; Wang, P. S. P.; Yan, E. C. Y. Parathyroid Hormone Senses Extracellular Calcium to Modulate Endocrine Signaling upon Binding to the Family B GPCR Parathyroid Hormone 1 Receptor. *ACS Chem Biol* **2018**, *13* (8), 2347–2358. <https://doi.org/10.1021/acscchembio.8b00568>.
- (35) Zhao, L. hua; Yuan, Q. ning; Dai, A. tao; He, X. heng; Chen, C. wei; Zhang, C.; Xu, Y. wei; Zhou, Y.; Wang, M. wei; Yang, D. hua; Xu, H. E. Molecular Recognition of Two Endogenous Hormones by the Human Parathyroid Hormone Receptor-1. *Acta Pharmacol Sin* **2022**, No. November, 1–11. <https://doi.org/10.1038/s41401-022-01032-z>.
- (36) Kobayashi, K.; Kawakami, K.; Kusakizako, T.; Miyauchi, H.; Tomita, A.; Kobayashi, K.; Shihoya, W.; Yamashita, K.; Nishizawa, T.; Kato, H. E.; Inoue, A.; Nureki, O. Endogenous Ligand Recognition and Structural Transition of a Human PTH Receptor. *Mol Cell* **2022**, *82* (18), 3468–3483.e5. <https://doi.org/10.1016/j.molcel.2022.07.003>.
- (37) Sozen, T.; Ozisik, L.; Calik Basaran, N. An Overview and Management of Osteoporosis. *Eur J Rheumatol* **2017**, *4* (1), 46–56. <https://doi.org/10.5152/eurjrheum.2016.048>.
- (38) Orloff, L. A.; Wiseman, S. M.; Bernet, V. J.; Fahey, T. J.; Shaha, A. R.; Shindo, M. L.; Snyder, S. K.; Stack, B. C.; Sunwoo, J. B.; Wang, M. B. American Thyroid Association Statement on Postoperative Hypoparathyroidism: Diagnosis, Prevention, and Management in Adults. *Thyroid* **2018**, *28* (7), 830–841. <https://doi.org/10.1089/thy.2017.0309>.
- (39) Rejnmark, L.; Underbjerg, L.; Sikjaer, T. Hypoparathyroidism: Replacement Therapy with Parathyroid Hormone. *Endocrinology and Metabolism* **2015**, *30* (4), 436–442. <https://doi.org/10.3803/EnM.2015.30.4.436>.

- (40) Rubin, M. R. et al. Therapy of Hypoathyroidism with Intact Parathyroid Hormone. *Osteoporos Int*. 21 (11), 1–7. <https://doi.org/10.1007/s00198-009-1149-x>. Therapy.
- (41) Winer, K. K.; Zhang, B.; Shrader, J. A.; Peterson, D.; Smith, M.; Albert, P. S.; Cutler, G. B. Synthetic Human Parathyroid Hormone 1-34 Replacement Therapy: A Randomized Crossover Trial Comparing Pump versus Injections in the Treatment of Chronic Hypoparathyroidism. *Journal of Clinical Endocrinology and Metabolism* **2012**, 97 (2), 391–399. <https://doi.org/10.1210/jc.2011-1908>.
- (42) White, A. D.; Jean-Alphonse, F. G.; Fang, F.; Peña, K. A.; Liu, S.; König, G. M.; Inoue, A.; Aslanoglou, D.; Gellman, S. H.; Kostenis, E.; Xiao, K.; Vilaradaga, J. P. Gq/11-Dependent Regulation of Endosomal CAMP Generation by Parathyroid Hormone Class B GPCR. *Proc Natl Acad Sci U S A* **2020**, 117 (13), 7455–7460. <https://doi.org/10.1073/pnas.1918158117>.
- (43) Malik, R. U.; Ritt, M.; DeVree, B. T.; Neubig, R. R.; Sunahara, R. K.; Sivaramakrishnan, S. Detection of G Protein-Selective G Protein-Coupled Receptor (GPCR) Conformations in Live Cells. *Journal of Biological Chemistry* **2013**, 288 (24), 17167–17178. <https://doi.org/10.1074/jbc.M113.464065>.
- (44) Semack, A.; Sandhu, M.; Malik, R. U.; Vaidehi, N.; Sivaramakrishnan, S. Structural Elements in the Gas and Gβq C Termini That Mediate Selective G Protein-Coupled Receptor (GPCR) Signaling. *Journal of Biological Chemistry* **2016**, 291 (34), 17929–17940. <https://doi.org/10.1074/jbc.M116.735720>.
- (45) Haimm, H. E.; Deretic, D.; Arendt, A.; Hargrave, P. A.; Koenig, B.; Hofmann, K. P. *Site of G Protein Binding to Rhodopsin Mapped with Synthetic Peptides from the α Subunit*. [www.sciencemag.org](http://www.sciencemag.org).
- (46) Kim, K.; Paulekas, S.; Sadler, F.; Gupte, T. M.; Ritt, M.; Dysthe, M.; Vaidehi, N.; Sivaramakrishnan, S. B2-Adrenoceptor Ligand Efficacy Is Tuned by a Two-Stage Interaction with the Gas C Terminus. *Proc Natl Acad Sci U S A* **2021**, 118 (11), 1–11. <https://doi.org/10.1073/pnas.2017201118>.
- (47) Culhane, K. J.; Gupte, T. M.; Madhugiri, I.; Gadgil, C. J.; Sivaramakrishnan, S. Kinetic Model of GPCR-G Protein Interactions Reveals Allosteric Modulation of Signaling. *Nat Commun* **2022**, 13 (1), 1–9. <https://doi.org/10.1038/s41467-022-28789-5>.
- (48) Sadler, F.; Ma, N.; Ritt, M.; Sharma, Y.; Vaidehi, N.; Sivaramakrishnan, S. Autoregulation of GPCR Signalling through the Third Intracellular Loop. *Nature* **2023**, 615 (March). <https://doi.org/10.1038/s41586-023-05789-z>.
- (49) Papasergi-scott, M. M.; Pérez-hernández, G.; Batebi, H.; Gao, Y.; Eskici, G.; Kobilka, B. K.; Hildebrand, P. W.; Skiniotis, G. Time-Resolved Cryo-EM of G Protein Activation by a GPCR. **2023**, No. Md, 1–43.
- (50) Hauser, A. S.; Kooistra, A. J.; Munk, C.; Heydenreich, F. M.; Veprintsev, D. B.; Bouvier, M.; Babu, M. M.; Gloriam, D. E. GPCR Activation Mechanisms across Classes and Macro/Microscales. *Nat Struct Mol Biol* **2021**, 28 (11), 879–888. <https://doi.org/10.1038/s41594-021-00674-7>.
- (51) Gao, Z. G.; Ijzerman, A. P. Allosteric Modulation of A2A Adenosine Receptors by Amiloride Analogues and Sodium Ions. *Biochem Pharmacol* **2000**, 60 (5), 669–676. [https://doi.org/10.1016/S0006-2952\(00\)00360-9](https://doi.org/10.1016/S0006-2952(00)00360-9).
- (52) *Phosphosite 7TM Antibodies*. <https://7tmantibodies.com/phosphosite-7tm--antibodies?p=1> (accessed 2023 -02 -15).

- (53) Sarkar, K.; Joedicke, L.; Westwood, M.; Burnley, R.; Wright, M.; McMillan, D.; Byrne, B. Modulation of PTH1R Signaling by an ECD Binding Antibody Results in Inhibition of  $\beta$ -Arrestin 2 Coupling. *Sci Rep* **2019**, *9* (1), 1–14. <https://doi.org/10.1038/s41598-019-51016-z>.